國 立 交 通 大 學

土木工程學系

博士論文

含材料變異自由樑在頻率量測誤差下之多裂縫診斷

Multiple Cracks Identification of Free-Free Beam with Uniform Material Property Variation and Noised Frequency Measurement

研 究 生：林 仁 正

指導教授：鄭 復 平　博士

中華民國 九十八 年 六 月

含材料變異自由樑在頻率量測誤差下之多裂縫診斷

Multiple Cracks Identification of Free-Free Beam with Uniform Material Property Variation and Noised Frequency Measurement

研究生：林仁正　　Student: Ren-Jeng Lin

指導教授：鄭復平 博士　　Advisor : Dr. Fu-Ping Cheng

國立交通大學

土木工程系

博士論文

A Dissertation

Submitted to Department of Civil Engineering

College of Engineering

National Chiao Tung University

In Partial Fulfillment of the Requirements

For the Degree of Doctor of Philosophy

In

Civil Engineering Department

June 2009

Hsinchu, Taiwan, Republic of China

中華民國 九十八 年 六 月

含材料變異自由樑在頻率量測誤差下之多裂縫診斷

研究生: 林仁正　指導教授: 鄭復平 博士

國立交通大學
土木工程系

摘要

各種結構破壞診斷方法中，常採用有效的振動訊號來進行，但這些方法中甚少考慮材料變異因素，而這些變異可來自許多實務上的原因，也將影響振動訊號之內涵，進而誤導診斷及監測結果。 本研究提出一種破壞診斷統計模型，並以自由樑裂縫診斷例子驗證模型成效，其中模態曲率用來偵測裂縫位置，並以蒙地卡羅方法建立合適統計資料庫，再以含有量測誤差之實測模態頻率比對此統計資料庫，以獲得裂縫深度。研究中各測試例子之模態參數取自實際加工之鋼樑以及有限元素模擬分析結果，從各演算例子的結果可證明，本研究提出之結構破壞診斷統計模型，可具體說明在結構系統中楊式係數及質量密度同時變異條件下，引入量測模態頻率誤差情況，可有效進行多裂縫自由樑之裂縫數目及其位置之診斷。

關鍵詞：多裂縫，破壞診斷，樑，變異，蒙地卡羅

Multiple Cracks Identification of Free-Free Beam with Uniform Material Property Variation and Noised Frequency Measurement

Student: Ren-Jeng Lin Advisor : Dr. Fu-Ping Cheng

Department of Civil Engineering
College of Engineering
National Chiao Tung University

Abstract

It is common to apply damage-sensitive features from vibration response for structural damage assessment. Fewer damage identification algorithms have been taken into account the material variation. The material variation could be caused by many reasons in engineering practice, also there may exists certain level noise in measurement, these variations may affect the features used for structure monitoring and lead to an inaccurate damage assessment.

In this research the authors proposed a model to assess statistical structural damage of free-free beam structure. The modal curvature-base feature was used to identify crack location. The statistical database for damage severity assessment was build by applying the Monte Carlo simulation with Latin hypercube sampling. By mapping vibration-sensitive features with noised modal frequency to statistical damage database, the damage probability among various crack depths were then estimated; its statistical significance of damage level were examined by the t-test.

Data from simulated beams and experimental modal analysis were used to demonstrate the assessment procedures. From the results, the authors concluded that the proposed algorithm was robust and able to identify the damage of free-free beam under uniform mass density and stiffness variations incorporated with noise in measured frequency.

Keywords: multiple cracks, damage assessment, beam, variation, Monte Carlo

誌謝

首先必須感謝我的指導老師鄭復平博士，多年來持續的在論文研究、工作與事業上的關心、提點與指導，也才能促成各項論文研究、期刊投稿及最終的博士論文產出，子曰：師者所以傳道、授業、解惑也，我的老師當之如分，當學生的我也衷心感謝，日後仍將再向老師多方請益。在博士修學期間，鄭老師、劉俊秀、洪士林及黃炯憲諸位老師學識淵博，使我藉修課及討論過程中獲益良多，在此一併深深感謝。

值得特別提出的是，論文審查及口試期間，承蒙楊明放院長、劉俊秀教授、洪士林教授、康淵教授及姜武英博士費心審度，其中提出許多重要觀點及後繼持續研究之重點，使本論文臻於完整，於此再次感謝。論文口試期間學弟妹們，多方關心及打理相關事務，一併致謝。

最後但仍很重要而必須一提的是，攻讀博士學位，來自家庭的全力支持，對於繁忙工作在身的我，許多家庭責任幾乎是單向傾斜於我內人身上，因此我很願意與我可愛的內人及兩個帥氣的兒子共享此項成果。

Contents

List of Tables

List of Figures

CHAPTER 1
Motivation, Literature Review, Research Approach and Coverage

1.1 Background and Motivation

The technique of Structural Health Monitoring (SHM) is to implement strategies of damage assessment for civil, aerospace, mechanical and other types of engineering structures. The damage is defined as the material properties loss or the geometric changes of systems which may include the boundary condition changes, the loss of component connectivity and material wear out so as to induce system performance degradation. In physical sense, a certain type of structure damage or material aging may cause the stiffness degradation in structure system and let the dynamic characteristics such as the modal frequency changed. Based on this assumption, a damage assessment algorithm may apply a specific damage-sensitive 'feature' from vibration signatures as an index to sense or to predict damage of the original healthy structure system.

It is also interesting that there may still other reasons to cause the dynamic characteristic or vibration signal changed which are not related to stiffness reduction from structure damage, one example for bridge structure, it could be gain or loss system weight due to environmental humidity to make the modal frequency changed. It should be the ultimate goal for the structure health monitoring strategy that it is capable of detecting a structure in damage situation, to locate the damage zone once the damage is happened and then to quantify the damage severity in a variant environment. In this research the authors apply simple beam structure as examples to develop a reliable and robust damage assessment algorithm and try to approach for this goal.

1.2 Statement of the Problems and Literature Review

Structure health monitoring has been received increasing interest in both of the academic research and industry applications for several decades [4]. An extensive literature review for 1975-1996 by Doebling et al. [8] was done at the Los Alamos national laboratory (LANL). The review focused on methods and data required for detecting, locating, and characterizing structure damage by examining the changes in various types of measured structure responses. The report also summarized state of the state of art of structural health monitoring technology and the applications by various damage identification methods for different types of structure. But almost none of the several hundred cited references took any statistical approach to access the damaged systems [28]. Another comprehensive updated literature review for 1996-2001 by Sohn et al. was also published by LANL [28]. The authors of the updated report mentioned that due to the observations of environment variability and operational conditions for long-term monitoring, the authors believe that structure health monitoring is a statistical pattern recognition problem fundamentally.

Sikorsky et al. [26] reported that there were 3.8% and 3.2% variations in first and second modal frequencies under 40℃ temperature variation over a 24-month observation for a bridge in Coachella Valley, California. Ko et al. [14] also recorded 12 months data from the cable stayed Ting-Kau bridge in Hong Kong and concluded that a 2.01% to 16.67% modal frequencies change occurred for the first 11 modes on about 50℃ temperature variation, and also the frequencies were decreased with increased temperature. Xia et al. [32] had constructed a reinforced concrete slab to investigate the correlations between vibration parameters and environment conditions. Data collected over 24 months showed there were 30℃ temperature and 65% humidity changes, and its frequencies had about 3% to 10% variations. The results also show that the frequencies decreased and damping ratio increased with the increased temperature and humidity. Other research also showed the same conclusion that the frequencies decreased as temperatures increased [6, 23, 27].

When environmental variability or operating condition is an important issue, it will affect the damage-sensitive features and may mask out real damage state and lead to inaccurate assessment. Xia et al. [32] advised that the vibration properties should be corrected to the same environmental conditions for structures in undamaged and damaged states. The same suggestion by Sohn et al. [28] was to do the data normalization so that the signal changes caused by variations can be separated from structural changes. Doebling and Farrar [9] are pioneers in examining the statistical significance of damage identification results using data collected on the I-40 highway bridge. Xia and Hao [31] assumed that the prior model and measure data fit for the Gaussian distribution and proposed a two-stage statistical identification algorithm. By taking the statistical operation of a second order Taylor's expansion on model updating equation, the authors estimated probability of damage existence by comparing the statistical distribution of element stiffness between undamaged and damaged states.

Furukawa and Otsuka [13] removed the Gaussian distribution assumption on variability and measurement noise, and then identified the possible damage of elements by the frequency response function changes from intact state deterministically. Then, they adopted the hypothesis test based on bootstrap re-sampling technique [10] to exclude the undamaged elements from the damaged element candidates. By iterative zoom-in process, the satisfied results will be obtained within 3 iterations for a large simulated system with 10% noise. Lin and Cheng [15] [16] proposed a algorithm and studied the beam structure with stiffness and mass variations to caused frequencies variation, by the Latin hypercube sampling technique in Monte Carlo simulation to assess crack location and severity statistically.

In the study of Oh and Sohn [18], they constructed a 5-layer AR-ARX neural network to extract the damage-sensitive features from measured time signals, then to apply the nonlinear principal component analysis to characterize the nonlinear relationship between unmeasured environmental and operational parameters.

Finally a hypothesis test named sequential probability ratio test is performed on the extracted feature to evaluate the damage state of the structure system. The proposed method is demonstrated by an eight-dof mass-spring example to show it is a promising data normalization tool and capable of detecting damage in the presence of environmental and operational variations with compared to another nonlinear principal component analysis realized by auto-associative neural network.

Bahlous et al. [2] developed a damage identification method to detect and locate damage, a normally distributed residual generated from modal filtering by the error calculating between current state measurements and their projections onto the incomplete modal basis of structure which is identified at reference state. The reinforced concrete beams and slabs samples which including multiple damage configurations were used to validate the proposed method. Despite the relative quantification errors of multiple damage scenarios are unacceptable in poor accuracy for locations, it's successful for the damage level less than 28% of the initial flexural stiffness.

Park et al. [22] apply time-modal features and two sequential artificial neural networks to detect damage in beam. The sequential approach consists two phases, the first phase is using cross-covariance functions of acceleration signals measured from two sensors, an acceleration-based neural networks algorithm is then designed to monitor the occurrence of damage in a structure. For the second phase, a modal feature-based neural networks algorithm is used to estimate the location and severity of damage in the structure by its mode shapes and modal strain energies. An Aluminum free–free beam and simply supported numerical beam samples are used to study for the feasibility of the proposed methodology

Rizos et al. [25] employ statistical estimation and hypothesis testing procedures to introduce two damage assessment methods which are capable of dealing with experimental uncertainty. The first method is a parametric model which

employs natural frequency and damping ratio interval estimates. The second method is a non-parametric model to apply coherence function interval estimates. Results of a stiffened aircraft panel were studied to indicate the feasibility of the methodology for both of damage detection and quality assessment of restoration.

Deraemaeker et al. [7] dealing with the problem of damage detection under changing environments by adopting two types of features which are extracted from the output-only vibration measurements by using automated stochastic subspace identification procedure and the peak indicators computed on the Fourier transform of modal filters. A numerical example of a bridge subject to environmental changes and damage is presented. The sensitivity of the damage detection procedure to noise on the measurements, environment and damage is studied. The estimation of the computational effort and the advantages and drawbacks of each of the features were studied and summarized in tables.

Wang and He [30] studied the natural frequencies reduction due to prescribed crack existence in arch dam and then build a statistical neural network to detect for the crack through measured natural frequencies. The crack can be detected by using the statistical neural network by the demonstration of simulated finite element model and a 1/100 scale concrete arch dam. Zhang [33] comments the inherent uncertainties in measurements is one of the main barriers against the application of vibration-based damage identification techniques on real bridges. A four steps statistical damage identification procedure for bridge health monitoring is then presented. The study of effectiveness and robustness of the proposed method is demonstrated by a numerical simulated three-span continuous girder bridge with reasonable damage severity.

A closed form derivation of statistical damage identification algorithm has many good aspects. However, for a complex system there may have difficulties, one example being to derive the distribution types of element stiffness for significant verification [31]. Instead, the fast development of computer hardware

made the computation intensive algorithm possible. Due to the uncertainty of related analysis of complex systems, Monte Carlo technique [24] was the simplest and most widely employed method. With the modification to Monte Carlo techniques, the Latin hypercube sampling (LHS) [17, 29] provided an efficient way of sampling variables with its distributions by assuming that all the variables are independent each other. Its efficiency are different from in diverse applications, some research reported that it saved more than 50% of computer effort [19]. Besides, compared to re-derivation of rigorous statistical damage identification algorithm, there is less effort spent and it is more intuitive to incorporate the well-developed deterministic damage identification algorithm with Monte Carlo based simulation technique.

1.3 Objectives, Approach and Research Coverage

By above discussions, we can conclude that the environment variability and operational conditions may play an important role in the accuracy, reliability and robustness in health monitoring process. The authors then aim at the development of a statistical damage assessment approach with considering the uniform mass and stiffness variability in system and also the possible frequencies measurement inaccuracy.

In the research, to extend the authors previous study work [15] [16], by assuming the environmental variability will cause the stiffness and mass variation on the entire beam uniformly, but no direct relate to temperature changes. The authors build up the statistical damage reference database which was incorporated with various property variations and damage states by applying the LHS techniques. And then to assess the statistical significance by applying the vibration features of an unknown damaged state and to use the t-test [12] to identify its damage locations. At last, the damage probability among the possible severity was estimated by mapping the vibration features to the statistical damage database. A

flowchart for the damage assessment procedures is presented in Fig. 1. Several demonstration examples showed that this approach was capable and robust to identify the damage of beam structure.

In the research, the authors have completed the study on below topics:

(1) To design for real cracked beam samples for benchmark samples to verify assessment algorithm proposed
(2) The formulation of simulated cracked beam for the study of vibration characteristic and to use for the build up a reference database for crack location detection and the crack extent assessment
(3) The setup of modal testing environment for the study the dynamic characteristic of real cracked beam
(4) To apply modal testing data as a reference for the correlation of simulated cracked beam to verify the capability of simulated beam formulation
(5) To abstract meaningful vibration features from both of the real cracked beam and simulated beam for crack identification and assessment
(6) To study the influence of uniform material variation from these vibration features and also study for how it affect the crack detection algorithm
(7) To propose a statistical model and process for the identification of property variation cracked beam under noise natural frequency measurement
(8) To review for the accuracy and robustness of proposed assessment model

1.4 Dissertation Outline

For chapter one the authors describe the general background of structure health monitoring and pointing out what is important but missed topic after paper review work, then raising the research objectives, approaches and research coverage.

In chapter two, to apply the singularity finite element for cracked beam and then to abstract its modal frequencies and mode shapes for later on database building. Effort also spend on the design of single and multiple cracked beam hardware for the verification of simulated cracked beam model and the benchmark hardware examples used in later.

There are two highlights in chapter three. One is the short introduction of experimental modal testing and the instrumentation used in our research, the other one is to do the results comparison between experimental modal testing and simulation to assure the modeling error in our research.

In chapter four, there will be a description for the procedures of damage assessment of multiple cracks beam for property invariant/variant system with/without noised modal frequencies. Also to present the abstraction of effective dynamic features (FCI and LDI) and the Influences study on the variation of stiffness and mass density.

Verification examples which are including the multiple cracks, a shallow crack and the effect on measurement resolution were studied in chapter five to demonstrate that the presented approach was capable and robust to identify the damage of beam structure with uniform mass and stiffness variations under the noise polluted frequency measured. Finally, the authors deliver conclusions and discussions regarding this research in chapter six.

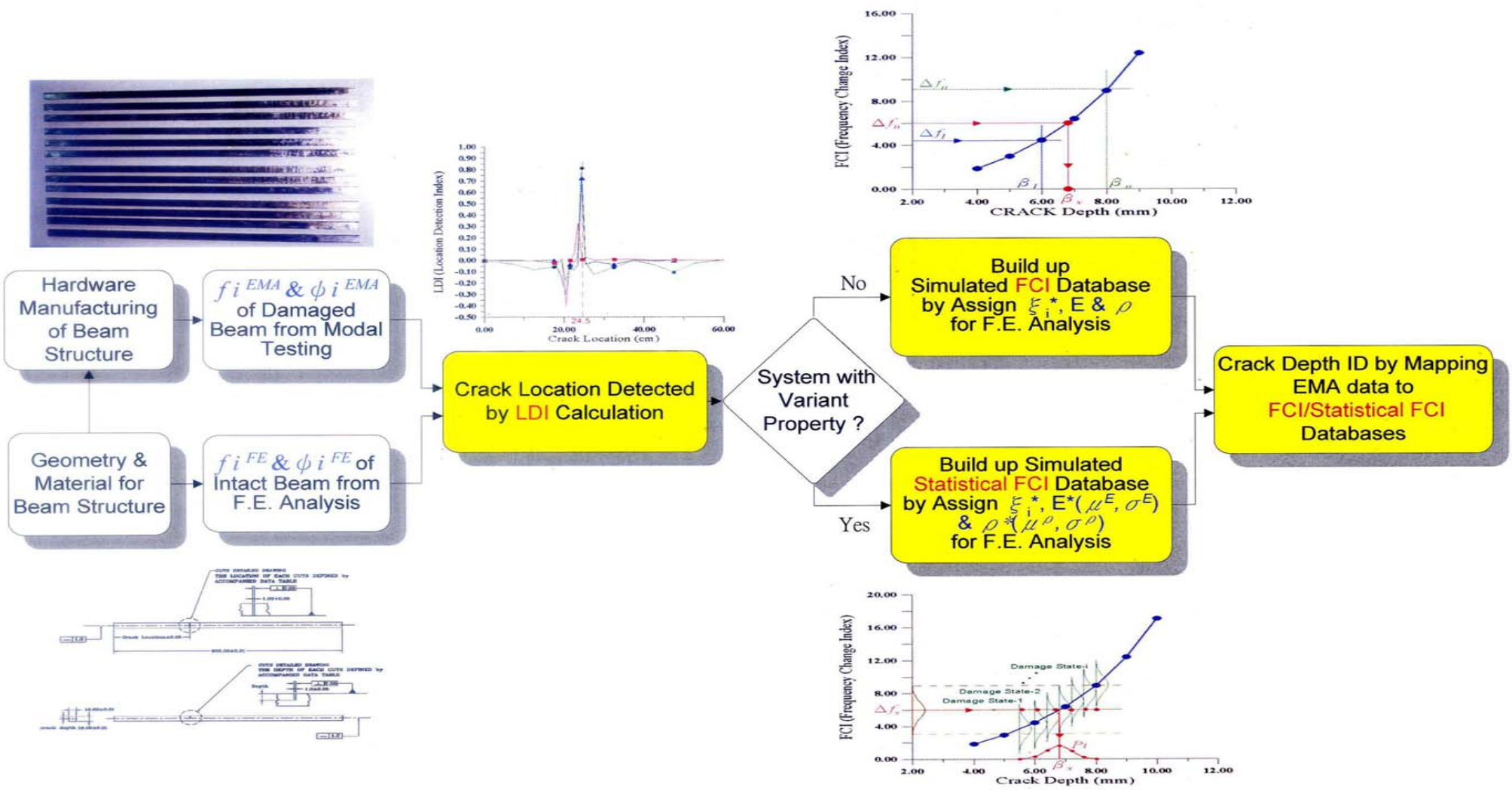

Figure 1. Flowchart of crack assessment procedures of beam structure

CHAPTER 2
Finite Element Modeling of Cracked Beam

In this chapter several topics will discussed so as to build a correct simulated crack-beam model, it will cover (1) to conduct the general element stiffness by finite element formulation from classical virtual work theory, (2) to introduce the crack tip singularity by quadratic iso-parametric element, and (3) the normal mode analysis of cracked beam. Also to introduce the design and accurate manufacturing of sample beam hardware for the later verification on the proposed damage assessment algorithm.

2.1 The Finite Element Method

For a general structure system with the body force and the traction on surface boundary, by the virtual work theorem [35], the internal strain energy is equal to the external work, hence we have the equation as below

$$\int_{vol} \delta\{\varepsilon\}^T \{\sigma\} d(vol) = \int_{vol} \delta\{u\}^T \{b\} d(vol) + \int_{area} \delta\{u\}^T \{t\} d(area) \quad (2.1)$$

Where

$\{\varepsilon\}$: Strain vector

$\{\sigma\}$: Stress vector

$\{u\}$: Displacement vector

$\{b\}$: Body force vector

$\{t\}$: Boundary traction vector

In general, we apply shape functions $[N_i]$ to interpret the displacement field with nodal coordinate, and also by the strain-displacement operator $[B_i]$ to link the relationship between strain and displacement as below equations:

$$\{u\} = [N_i]\{d_i\} \qquad \{\delta u\} = [N_i]\{\delta d_i\}$$

$$\{\varepsilon\} = [B_i]\{d_i\} \qquad \{\delta\varepsilon\} = [B_i]\{\delta d_i\} \tag{2.2}$$

Where

d_i : Nodal displacement vector

δd_i : The virtual nodal displacement vector

$[N_i] = [I]N_i$: The matrix of prescribe function in global form

$[B_i]$: The global strain-displacement function

By appropriate arrangement, we have Eq. (2.3)

$$\{\delta d_i\}^T \left\{ \int_{vol} [B_i]^T \{\sigma\} d(vol) - \int_{vol} [N_i]^T \{b\} d(vol) - \int_{area} [N_i]^T \{t\} d(area) \right\} = 0 \tag{2.3}$$

The necessary condition to satisfy non-trivial solution for Eq. (2.3) written as below,

$$\int_{vol} [B_i]^T \{\sigma\} d(vol) - \int_{vol} [N_i]^T \{b\} d(vol) - \int_{area} [N_i]^T \{t\} d(area) = 0 \tag{2.4}$$

Also the stress is interrelated with strain by the elasticity matrix,

$$\{\sigma\} = [D]\{\varepsilon\} = [D][B_i]\{d_i\} \tag{2.5}$$

Insert Eq. 2.5 into Eq. 2.4, we have Eq. 2.6

$$[K]\{d_i\} = \int_{vol} [N_i]^T \{b\} d(vol) + \int_{area} [N_i]^T \{t\} d(area) \tag{2.6}$$

Where

$$[K] = \int [B_i]^T [D] [B_j] d(vol) \tag{2.7}$$

2.2 Singularity Element for Cracked Zone

Cracked beam formulation will deal with the cracked tip and the intact zone modeling. Thick shell elements [34] were used for the intact zone. For the cracked zone, the authors applied the thick shell elements combined with degenerated quarter point singularity formulation [3]. In the research only the $1/\sqrt{r}$ singularity will be studied, it needs further research effort for other order singularity.

The most convenient way to introducing a $1/\sqrt{r}$ strain singularity into a quadratic iso-parametric element is to manipulate the mid-side node position to 1/4 length along the two edges which are nearby crack tip node. Consider the quadratic iso-parametric element shown in Fig. 2 in which the nodal points are locally numbered as 1 to 8.

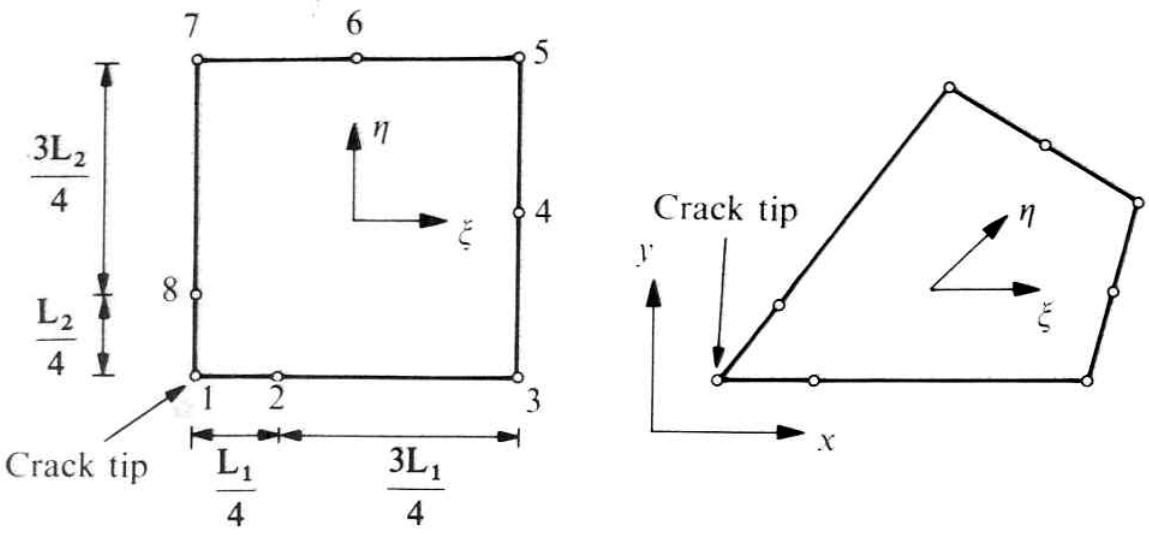

Figure 2. Quadratic iso-parametric element with mid-side nodes at the quarter point [20]

The corner nodes' shape function of quadratic iso-parametric element can be expressed as:

$$N_i^{(e)} = \frac{1}{4}(1+\xi\xi_i)(1+\eta\eta_i)(\xi\xi_i + \eta\eta_i - 1) \tag{2.8}$$

For the middle node's shape function are expressed as:

$$N_i^{(e)} = \frac{1}{2}\xi_i^2(1+\xi\xi_i)(1-\eta^2) + \frac{1}{2}\eta_i^2(1+\eta\eta_i)(1-\xi^2) \tag{2.9}$$

Defining the shape function of edge 1-3 by assign $\eta_i = -1$ and associate ξ_i, η_i into equation Eqs. (2.8) and (2.9) we will have shape functions of node 1 to 3 as follow,

$$\begin{aligned} N_1 &= -\frac{1}{2}\xi(1-\xi) \\ N_2 &= (1-\xi^2) \\ N_3 &= \frac{1}{2}\xi(1+\xi) \end{aligned} \tag{2.10}$$

To insert Eq. (2.10) into $x = \sum_{i=1}^{3} N_i x_i$, we have displacement along edge 1-3, or node 1, 2 and 3 by below equation,

$$x = \sum_{i=1}^{3} N_i x_i = -\frac{1}{2}\xi(1-\xi)x_1 + (1-\xi^2)x_2 + \frac{1}{2}\xi(1+\xi)x_3 \tag{2.11}$$

To introduce the desire singularity at node 1 by moving mid-point node 2 to the quarter point position as shown in Fig. 2. Denoting the length along edge 1-3 is L_1, then x_2 for node 2 would be $L_1/4$, and $x_1 = 0$, $x_3 = L_1$, by inserting these numbers to Eq. (2.11) we have Eq. (2.12)

$$x = \frac{1}{2}\xi(1+\xi)L_1 + (1-\xi^2)\frac{L_1}{4} \tag{2.12}$$

Or we have the non-trivial root,

$$\xi = -1 + 2\sqrt{\frac{x}{L_1}} \tag{2.13}$$

The result in Eq. (2.13) will apply to the $\frac{\partial u}{\partial x}$ calculation in Jacobian matrix operation to get the element stiffness matrix which will let node 1 posses the strain singularity [20]. And we will have the displacement along the edge of node 1-3 as below

$$u = \sum_{i=1}^{3} N_i d_i = -\frac{1}{2}\xi(1-\xi)u_1 + (1-\xi^2)u_2 + \frac{1}{2}\xi(1+\xi)u_3 \tag{2.14}$$

To insert Eqs. (2.13) into (2.14) we also have the displacement function as below

$$u = -\frac{1}{2}\left[-1+2\sqrt{\frac{x}{L_1}}\right]\left[2-2\sqrt{\frac{x}{L_1}}\right]u_1 + 4\left[\sqrt{\frac{x}{L_1}} - \frac{x}{L_1}\right]u_2 + \frac{1}{2}\left[-1+2\sqrt{\frac{x}{L_1}}\right]\left[2\sqrt{\frac{x}{L_1}}\right]u_3 \tag{2.15}$$

Then the strain in x direction will be

$$\varepsilon_x = \frac{\partial u}{\partial x} = -\frac{1}{2}\left(\frac{3}{\sqrt{xL_1}} - \frac{4}{L_1}\right)u_1 + \left(\frac{2}{\sqrt{xL_1}} - \frac{4}{L_1}\right)u_2 + \frac{1}{2}\left(-\frac{1}{\sqrt{xL_1}} + \frac{4}{L_1}\right)u_3 \tag{2.16}$$

We observe that the strain singularity along edge 1-3 is therefore in the required order $1/\sqrt{r}$, by the same process we can also generate strain singularity along the edge 1-7 which is related to ε_y.

However, the strain variation is not of the form $1/\sqrt{r}$ within the element along the rays of edge 1-3 and 1-7 which are emanating from node 1. Such of this condition can be enforced by forming a triangular element by 'collapsing' the edge which is consists of nodes 1, 7, and 8 and shown in Fig. 3.

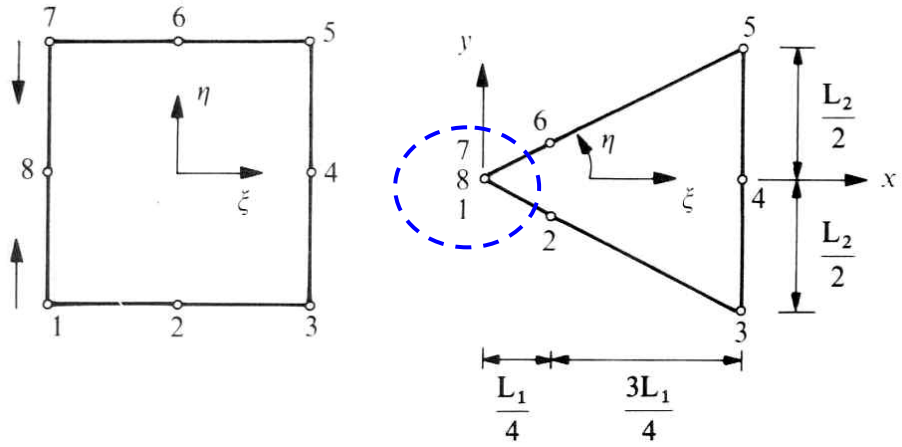

Figure 3. Triangular element with mid-side nodes at the quarter point [20]

Again, we move the mid-side nodes 2 and 6 to the quarter point adjacent to the crack tip, node 1, which is considered as the coalesced node. Locating the originate node at node 1, we have

$$\begin{aligned} x_1 &= x_7 = x_8 = 0 \\ x_2 &= x_6 = L_1/4 \\ x_3 &= x_4 = x_5 = L_1 \end{aligned} \tag{2.17}$$

And the shape functions are

$$\begin{aligned} N_1 &= N_3 = N_5 = N_7 = -\frac{1}{4}\left(1-\xi^2\right) \\ N_2 &= N_6 = \frac{1}{2}\left(1-\xi^2\right) \\ N_4 &= N_8 = \frac{1}{2}\left(1-\xi\right) \end{aligned} \tag{2.18}$$

By inserting Eqs. (2.17) and (2.18) into $x = \sum_i N_i x_i$, we have

$$x = \frac{L_1}{4}(1+\xi)^2 \tag{2.19}$$

Or that

$$\xi = -1 + 2\sqrt{\frac{x}{L_1}} \tag{2.20}$$

The displacement distribution along the x axis is from Eq. (2.18) and $u = \sum_i N_i d_i$

$$u = -\frac{1}{4}(1-\xi^2)(u_1 + u_3 + u_5 + u_7) + \frac{1}{2}(1-\xi^2)(u_2 + u_6) + \frac{1}{2}(1-\xi)(u_4 + u_8) \tag{2.21}$$

Denoting $u_1 = u_7 = u_8$, and the strain distribution is,

$$\varepsilon_x = \frac{\partial \xi}{\partial x}\frac{\partial u}{\partial \xi} = \frac{1}{L_1}(2u_1 + u_3 + u_5 - 2u_2 - 2u_6) - \frac{1}{2\sqrt{L_1 x}}(3u_1 + u_3 + u_4 + u_5 - 2u_2 - 2u_6) \tag{2.22}$$

The strain component ε_x possesses a $1/\sqrt{r}$ singularity. It is more general to exhibit the $1/\sqrt{r}$ singularity for all the region along the 'ray' emanating from cracked tip node with compare to singularity only happened on the two edges for the quadrilateral element version.

2.3 Normal Mode Analysis of Cracked Beam

In this research, the authors proposed a model to assess statistical structural damage by applying the modal curvature-base feature to identify crack location and also to apply the modal frequency to identify crack depth of beam structure. For the damage assessment process, the modal frequency and mode shape abstraction were required to produce these damage-sensitive features.

The real eigen-value normal mode analysis is the basis of linear structure dynamic analysis. The mass and stiffness elements were used to construct the below dynamic equation.

$$[M]\{\ddot{u}(t)\}+[K]\{u(t)\}=\{0\} \tag{2.23}$$

Assume the solution is in the form of

$$\{u(t)\}=\{\tilde{u}\}\sin\left(\omega t+\theta\right) \tag{2.24}$$

Where

[M]、[K]: The system mass and stiffness matrices

$\{u(t)\}$: Displacement vector along time

ω : The circular natural frequency of structure system

θ : The phase angle among different modes

$\tilde{u}$: The shape of dynamic system which is time independent

By the differentiation twice of Eq. (2.24), we have

$$\{\ddot{u}(t)\}=-\omega^2\{\tilde{u}\}\sin\left(\omega t+\theta\right)=-\omega^2\{u(t)\} \tag{2.25}$$

To substitute Eqs. (2.24) and (2.25) into Eq. (2.23), we got Eq. (2.26)

$$-\omega^2[M]\{\tilde{u}\}\sin(\omega t+\theta)+[K]\{\tilde{u}\}\sin(\omega t+\theta)=\{0\} \tag{2.26}$$

Or that

$$([K]-\omega^2[M])\{\tilde{u}\}\sin(\omega t+\theta)=\{0\} \tag{2.27}$$

Below equation is the nontrivial solution if to let the determinant goes to zero, i.e.

$$\left\|[K]-\omega^2[M]\right\|=0 \tag{2.28}$$

Eq. (2.28) is called the frequency equation of system, to expand the determinant will give an Nth algebraic in the parameters of ω for the N degree of freedom dynamic system. Its N roots represent the normal frequency of the N modes in the system.

There are two ways to construct the mass matrix [5], the lumped mass from simplest physical sense and the other is making use of finite element concept to apply the same shape function to generate consistent mass. The lumped mass is in diagonal matrix form whereas the consistent mass is presented in full matrix, hence more computational effort than the lumped mass system does. In this research the lumped mass form will be good enough for damage assessment purpose.

Regarding the stiffness matrix, as previous session described, there are two types of stiffness matrix need to handle, the general plate element stiffness by finite element formulation by Eq. (2.7) and also the second type element stiffness for cracked zone around crack tip, it should construct from a standard quadratic iso-parametric element by moving mid-point nodes to the quarter point position plus a ‘collapsing’ edge to exhibit the $1/\sqrt{r}$ singularity in entire element and around the crack tip.

Most commercial packages have provided the tool for normal mode analysis. In this research the authors apply ANSYS® as a template to deploy damage assessment algorithm. The result of a typical analysis for a two-crack beam was shown in Fig. 4. This cracked beam will also used as a demonstrate example for the proposed damage assessment algorithm in session 5.6.

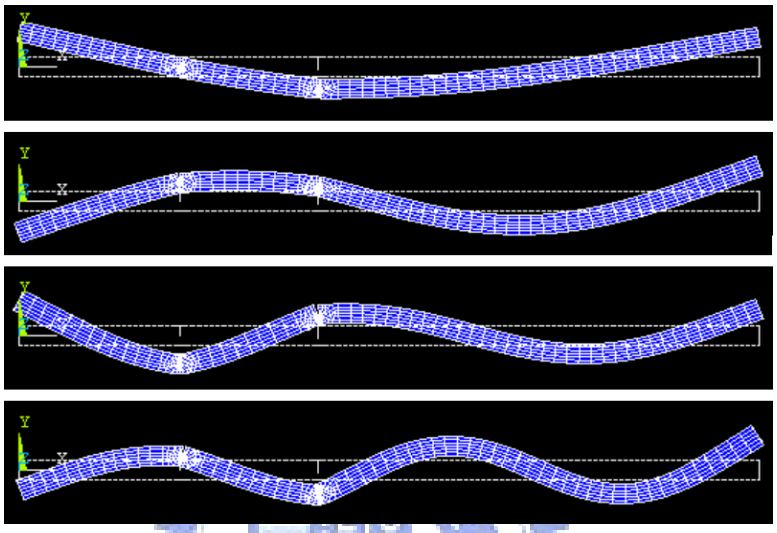

Figure 4. Typical normal mode analysis result of a two-crack beam

2.4 Configurations of the Cracked Sample Beams

In order to control the accuracy of demonstrate sample beams and also for to verify the effectiveness of proposed damage assessment algorithm. The sample beams were well prepared by applying simulation before hardware manufacturing to determine its length and cross section to include three normal modes within 2KHz. There are all rectangular-sectioned mild steel bar, 600mm(L) x 16mm(W) x 16mm(H) in size, all the artificial cracks were made by high accurate wire-cut with 0.50mm slot width on specific crack location and planned crack depth.

There are total 15 sample beams which can be separated in two categories, the configuration and drawing of sample beams were shown in Table 1, Fig. 5 and 6. One group was the intact beam (beam-S). The others were with artificial cracked and named from A to N, all these beams were single cracked, except beam-M with 2 cracks and designed for the multiple cracks assessment purpose.

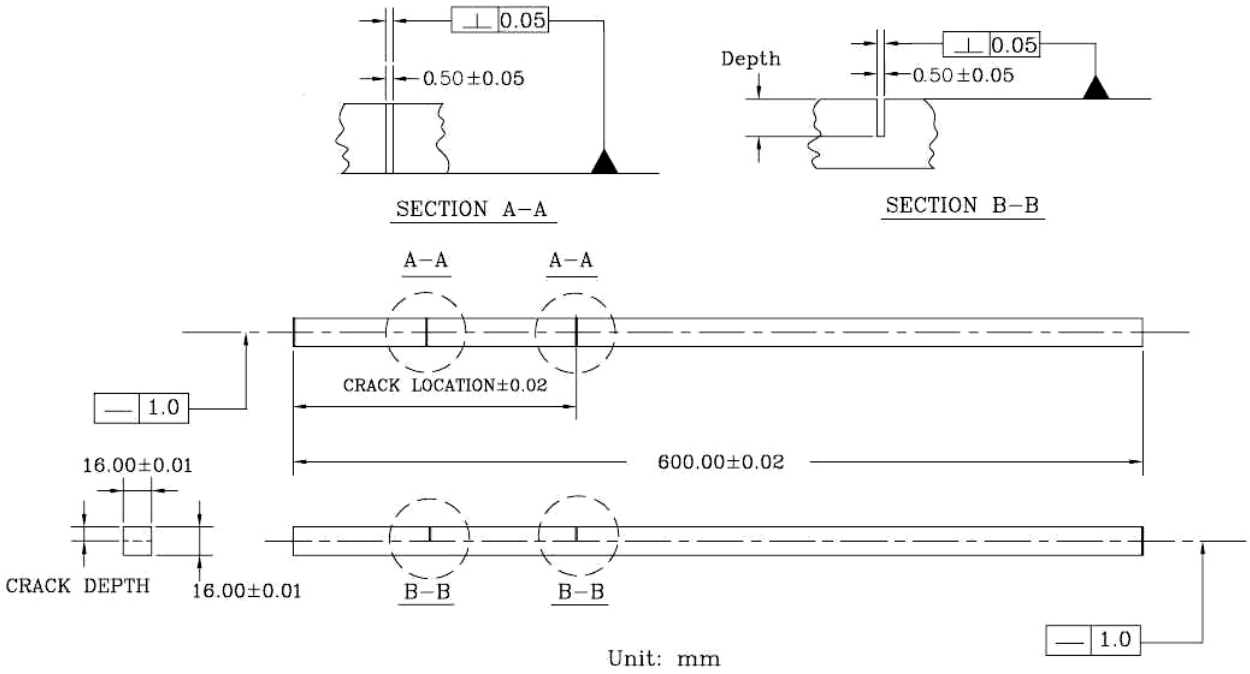

Figure 5. Drawing of the crack beam sample

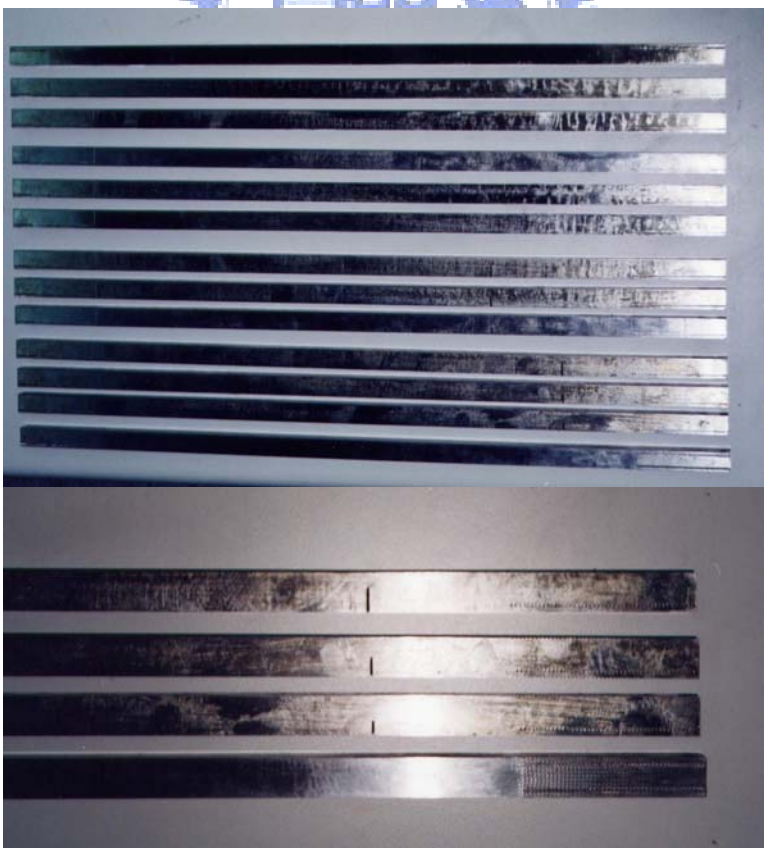

Figure 6. Photo of crack beam samples

Table 1 Configuration of sample beams

Sample No.	Sample Name	1st Crack (Loc., Depth) (Unit in mm)	2nd Crack (Loc., Depth) (Unit in mm)	Remark
1	A	(131.0, 6.0)	None	
2	B	(131.0, 8.0)	None	
3	C	(131.0, 10.0)	None	
4	D	(187.0, 6.0)	None	
5	E	(187.0, 8.0)	None	
6	F	(187.0, 10.0)	None	
7	N	(243.0, 3.0)	None	Shallow crack test example
8	G	(243.0, 6.0)	None	
9	H	(243.0, 8.0)	None	
10	I	(243.0, 10.0)	None	Resolution test example
11	J	(300.0, 6.0)	None	
12	K	(300.0, 8.0)	None	
13	L	(300.0, 10.0)	None	
14	M	(131.0, 8.0)	(243.0, 10.0)	Multi-crack test example
15	S	Intact Beam (without Damage)		Reference example

CHAPTER 3
Experimental Modal Analysis and the Simulation Results Comparison

In this chapter, the experimental modal analysis was discussed and the instrumentation of a PC base data acquisition system for hammer impact test was introduced, also the modal test results were compared with simulated cracked beam. By reviewing the results, the authors concluded that the simulation model and test setup is appropriate and accurate enough to process the verification work on the proposed damage assessment model.

3.1 Experimental Modal Analysis [11]

Modal testing is the techniques to perform vibration testing of an object, a mechanical component or a specific structure system. The investigation of dynamic characteristic are including the natural (modal) frequencies, modal mass, modal damping ratios and also the mode shapes. A modal test is consists of the acquisition instrumentation and the analysis algorithm as well. The complete process is often referred to as a Modal Analysis or Experimental Modal Analysis (EMA).

There are several ways to perform the modal testing. The most widely used is the impact hammer modal testing and the shaker modal testing. In both cases the energy is apply to the tested system with known frequency content. Wherever structural resonance occurs on certain frequency there will be accompanied with vibration amplification, a clearly sign in response spectra. There are many methods for modal parameter estimation, in mathematics viewpoint, a transfer function or so-call Frequency Response Function (FRF) can be obtained by the calculating on response spectra and force spectra, it is often completed by curve fitting to estimate the modal parameters.

The hammer test is the simplest way to perform modal testing. It is designed to replicate a perfect impulse impact to a structure, the impulse which has an infinitely small duration, causing constant amplitude in the frequency domain; this would result in all modes of vibration being excited with equal energy. However, in reality a hammer strike cannot last for an infinitely small duration, but has a known contact short time. The duration of the contact time directly influences the frequency content of the force, with a longer contact time will induce a smaller range of frequency bandwidth. A load cell is attached to the end of the hammer to obtain a recording of the force.

Impact hammer testing is ideal for small light weight structure system which is appropriate in academic research to study for the proposed damage assessment algorithm, however as the size of the studied structure system increases, other excitation and analysis method will be needed to improve the poor signal to noise ratio issue which is common on large civil engineering structures.

3.2 Frequency Response Function

The Frequency Response Function (FRF) can be used to define the input/output relation. For a general structure system, we have the dynamic equation as below:

$$m\ddot{u}(t) + c\dot{u}(t) + ku(t) = f(t) \tag{3.1}$$

If the impact force and system response is represented in frequency domain by the magnitude and phase angle, we can write the following relation.

$$f(t) = Fe^{i\omega t} \tag{3.2}$$

$$u(t) = Xe^{i\omega t} \tag{3.3}$$

Substitute Eqs. (3.1) and (3.2) in Eq. (3.3) we will have the transfer function in (3.4). H(ω) is called the FRF (also referred as the transfer function) and its magnitude

and phase angle $\phi(\omega)$ are represented in Eqs. (3.4) and (3.5).

$$H(\omega)=\frac{X(\omega)}{F(\omega)}=\frac{1}{\left(k-\omega^2 m\right)+i\omega c}=\frac{1}{k\left[\left(1-\frac{\omega^2}{\omega_n^2}\right)+2i\varsigma\left(\frac{\omega}{\omega_n}\right)\right]}$$

$$=\frac{1}{-\omega^2 m\left[\left(1-\frac{\omega^2}{\omega_n^2}\right)-2i\varsigma\left(\frac{\omega}{\omega_n}\right)\right]} \tag{3.4}$$

$$\phi(\omega)=\tan^{-1}\frac{2\varsigma\left(\frac{\omega}{\omega_n}\right)}{\left(1-\frac{\omega^2}{\omega_n^2}\right)} \tag{3.5}$$

Unlike the ideal structure simulation by computer, for the modal testing measurement is usually incorporated with possible noise from instrumentation, nonlinear effect and limited frequency resolution, it can be improved by the random data analysis. Firstly, we introduce the correlation function defined in Eq. (3.6), and the correlation function $R_{xy}(\tau)$ and spectrum functions $G_{xy}(f)$ are the Fourier pair described in Eq. (3.7). The x and y suffix represented for the input and output signal respectively.

$$R_{xy}(\tau)=\lim_{x\to\infty}\int_{-t/2}^{t/2} f_x(t)f_y(t+\tau)d\tau \tag{3.6}$$

$$G_{xy}(f)=F\{R_{xy}(\tau)\}$$

$$R_{xy}(\tau)=F^{-1}\{G_{xy}(f)\} \tag{3.7}$$

H_1 in Eq. (3.8) transfer function is used to eliminate noise by the averaging of output signal, it will be more accurate to present the anti-resonance peak, where H_2 in Eq. (3.9) transfer function is accurate in the resonance peak due to it can only

eliminate noise by the averaging of input signal. The H_1 and H_2 transfer function are used to define the lower bound and upper bound of FRF curve respectively. Due to the hammer test is applied in well control lab, in this research, the H_1 will be used to prove for the proposed damage assessment algorithm.

$$H_1 = \frac{G_{xy}}{G_{xx}} = \frac{G_x G_y}{G_x G_x} \tag{3.8}$$

$$H_2 = \frac{G_{yy}}{G_{xy}} = \frac{G_y G_y}{G_x G_y} \tag{3.9}$$

Where

G_{xx} : The power spectrum of input signal

G_{yy} : The power spectrum of output signal

G_{xy} : The cross spectrum between input and output signal

G_x : The spectrum from Fourier integral of input signal

G_y : The spectrum from Fourier integral of output signal

In data acquisition phase by hammer impact, it is common to apply the Force window and Exponential window time domain weighting function to avoid the leakage phenomenon.

The Force window is used for hammer impact test which the time domain signal is started and ended to zero state, and it can improve the quality of input signal by eliminating noise while in improper movement or hammer contact during the impact operation. It can be defined as below equation.

$$\begin{aligned} \omega(t) &= 1 \qquad t_0 < T \\ \omega(t) &= 0 \qquad else \end{aligned} \tag{3.10}$$

The Exponential window is used to limit output signal to follow a natural decay trend and also improve the quality of time domain data. It can be defined in time domain by eq. (3.11) or in frequency domain by eq. (3.12)

$$\omega(t) = e^{-(t-t_0)/T} \quad t_0 < T \text{ and } 0 < t < T$$
$$\omega(t) = 0 \qquad else \tag{3.11}$$

$$L(f) = \frac{\tau}{1 + i2\pi f} = \frac{t - t_0}{1 + i2\pi f} \tag{3.12}$$

3.3 Experimental Instrumentation

There are three elements for the instrumentation of modal testing in this research, the excitation hammer, the sensing accelerometer, and data acquisition/analysis system. The data acquisition system is delivered by Prowave® Engineering Inc., it consists of a PC with a multi-channel AD/DA module (SC-612), a BNC I/O control box (PW-145), a real time control/analysis software (Signal Doctor) and the off-line modal parameter analysis software (STAR®).

The PCB 7375 hammer is used for impact excitation with a sensitivity 2.20mv/N, and the PCB 7684 accelerometer is used to sense vibration response, its sensitivity 10.43mv/g. The sensor and impact hammer is connected to the PC control system to get the excitation and response of beam. The PC base acquisition system shown in Fig. 7, and the parameters setting of hammer impact test system is shown in Fig. 8.

In order to match with the simulation free-free boundary condition, two rubber strings were used to suspend the sample beam as shown in Fig. 9. The sampling rate was set as 2000Hz, with 1.25Hz resolution, fixed sensor at one end of sample beam, 12 to18 locations were planned for hammer impact, and each location takes 10 times impact for average. A typical hammer test result is shown in Fig. 10.

Due to the density of impact locations will affect the resolution of mode shape and also the curvature mode shape for damage assessment, it will dominate the accuracy of assessment results which will discuss in later chapter. We should also noticed that for practical engineering the ‘fixed response’ method should be changed to ‘fixed impact’ to save the labor work.

Figure 7. The PC base data acquisition system

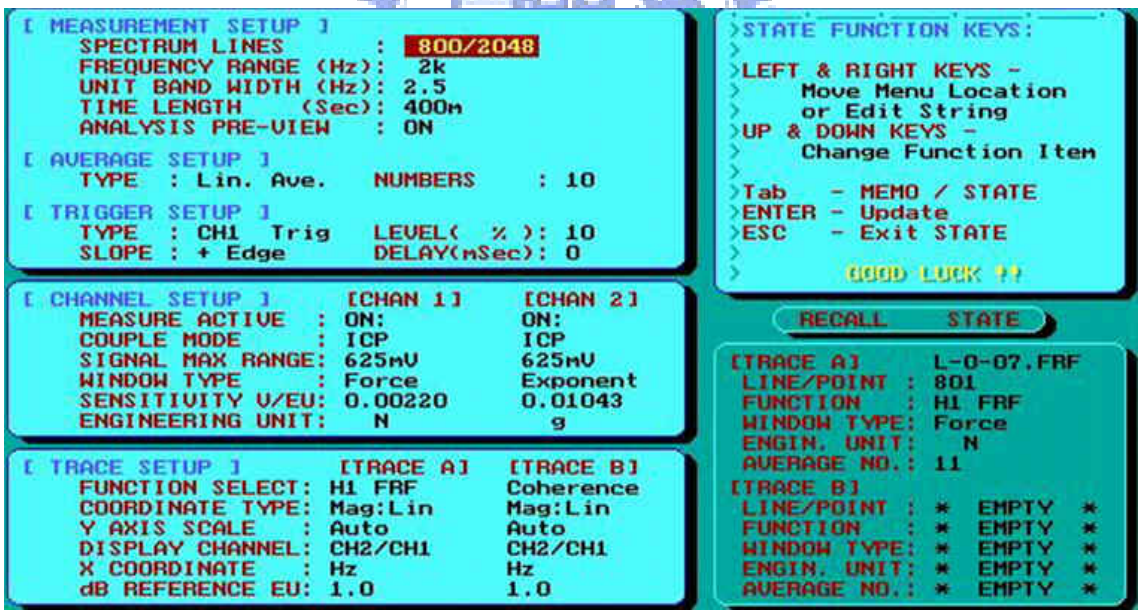

Figure 8. Parameters settings of hammer Impact testing

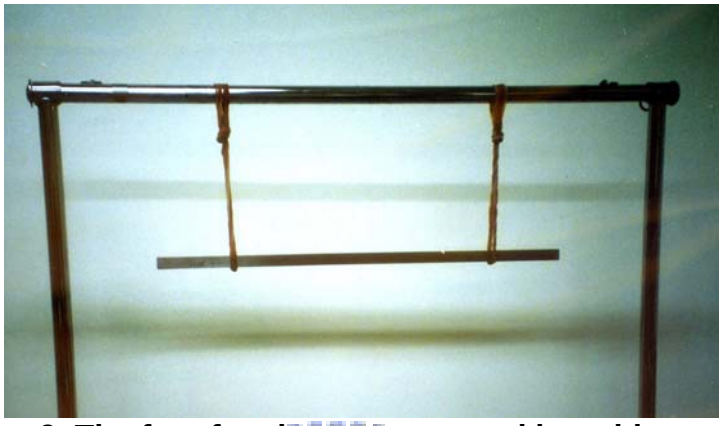

Figure 9. The free-free beam supported by rubber spring

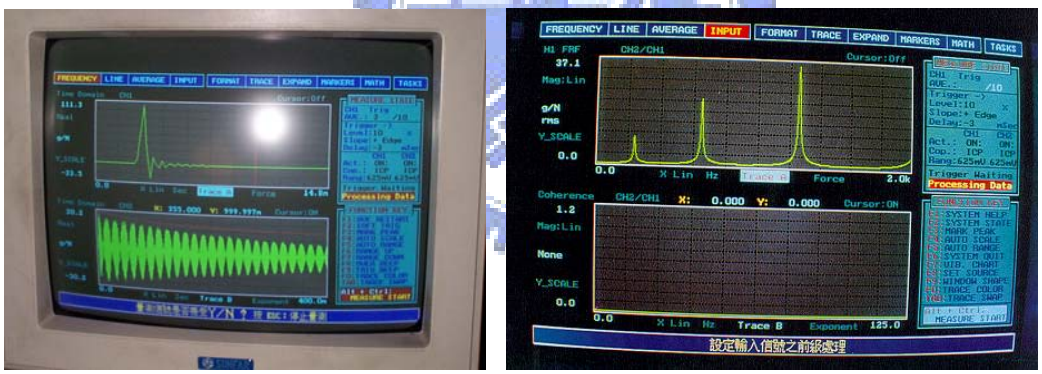

Figure 10. A typical test result for hammer impact test

3.4 Experimental and Simulation Results Comparison

An accurate prior model is essential for the supervised damage assessment algorithm [28]. In the session the authors is focus on the comparison results of simulated beam and the EMA test.

To review the results, we found it is consistent for simulation and EMA. The simulation results are accurate in frequencies and mode shapes among sample beams by refer to error statistics of frequency and mode shape in Table 2 and 3. Its mean error of modal frequencies was under 0.24% and the maximum error was under 0.78% for the lowest three modes.

Besides the frequency comparison, a comparison of mode shape plots between simulation & EMA for beam-S, I and F were shown in Fig. 11**,** in general, the modal assurance criterion (MAC) [1] was used to measure the accuracy of mode shapes between analytical and experimental models. When the MAC was closed to 1.0, the results have a good correlation and it was uncorrelated or in-accurate when the MAC was closed to 0.0. By combining the calculations of different mode shapes of analytical and experimental, we can construct the MAC in matrix form. From the calculation, we found the diagonal terms in MAC matrix were all larger than 0.997, and the off-diagonal terms were all under 0.064 for the lowest three modes for all sample beams.

It should noted that the error or uncertainty of finite element prior model can be included in the statistical model by assigning the variances of stiffness and mass directly.

Table 2. Frequencies comparison and error statistical between simulation and EMA

Sample Beam		Mode-1			Mode-2			Mode-3		
		Simulation (Hz)	EMA (Hz)	Error (%)	Simulation (Hz)	EMA (Hz)	Error (%)	Simulation (Hz)	EMA (Hz)	Error (%)
S		234.12	234.83	0.30	642.24	644.13	0.29	1250.30	1253.81	0.28
A		231.57	232.04	0.20	619.32	621.03	0.28	1197.97	1202.16	0.35
B		228.64	228.98	0.15	595.31	595.98	0.11	1153.93	1156.70	0.24
C		222.31	221.85	0.21	552.02	549.83	0.40	1093.93	1093.78	0.01
D		227.64	228.01	0.16	614.84	616.42	0.26	1238.53	1241.43	0.23
E		220.57	220.57	0.00	589.96	590.69	0.12	1228.59	1232.00	0.28
F		206.73	206.32	0.20	552.07	552.27	0.04	1214.36	1216.48	0.17
G		223.84	224.14	0.13	630.04	631.79	0.28	1238.40	1241.77	0.27
H		213.35	213.19	0.08	618.91	620.17	0.20	1227.32	1229.71	0.19
I		194.55	193.43	0.58	601.73	602.38	0.11	1209.56	1210.66	0.09
J		222.28	222.59	0.14	642.17	643.54	0.21	1204.28	1208.05	0.31
K		210.51	210.15	0.17	642.13	643.50	0.21	1164.18	1166.15	0.17
L		190.14	188.66	0.78	642.07	643.36	0.20	1105.24	1105.24	0.00
Error statistical (%)	Mean	0.2388			0.2085			0.2003		
	Min.	0.0000			0.0362			0.0000		
	Max.	0.7784			0.3983			0.3485		
	Deviation	0.2131			0.0962			0.1092		

Table 3. MAC comparison between simulations and EMA results

Sample Beam	MAC Matrix (for the lowest 3 modes)			Error Norm		
				Diagonal Terms	Off-Diagonal Terms	Over-all
S	0.9997556	0.0000195	0.0640758	0.0005110	0.0351383	0.0286918
	0.0000961	0.9995058	0.0000063			
	0.0574673	0.0000239	0.9993076			
A	0.9995185	0.0000657	0.0595545	0.0006913	0.0323707	0.0264336
	0.0000026	0.9993078	0.0002000			
	0.0523488	0.0000010	0.9991499			
B	0.9997178	0.0012808	0.0521253	0.0015762	0.0292249	0.0238793
	0.0002297	0.9991084	0.0000224			
	0.0490491	0.0000252	0.9974352			
C	0.9996556	0.0017986	0.0557174	0.0013714	0.0296133	0.0241922
	0.0004814	0.9983692	0.0000688			
	0.0464091	0.0000079	0.9983075			
D	0.9997057	0.0000009	0.0617004	0.0005378	0.0332398	0.0271420
	0.0000003	0.9996627	0.0000934			
	0.0531196	0.0008168	0.9991832			
E	0.9998214	0.0001395	0.0615837	0.0008113	0.0319949	0.0261279
	0.0000398	0.9994664	0.0008507			
	0.0484061	0.0023657	0.9987124			
F	0.9995707	0.0002938	0.0557912	0.0012282	0.0289113	0.0236167
	0.0000393	0.9993457	0.0025953			
	0.0430968	0.0061953	0.9980218			
G	0.9995372	0.0001081	0.0588879	0.0011971	0.0333857	0.0272680
	0.0002931	0.9991980	0.0000322			
	0.0567402	0.0005276	0.9981447			
H	0.9997761	0.0001236	0.0574464	0.0009098	0.0330438	0.0269853
	0.0005583	0.9993614	0.0000240			
	0.0570168	0.0001539	0.9985768			
I	0.9993042	0.0000796	0.0630813	0.0009374	0.0340169	0.0277799
	0.0007971	0.9991642	0.0001819			
	0.0544331	0.0000310	0.9987944			
J	0.9997957	0.0000075	0.0592480	0.0006385	0.0327852	0.0267715
	0.0000554	0.9996182	0.0000112			
	0.0542112	0.0001453	0.9989824			
K	0.9996760	0.0000006	0.0570203	0.0007496	0.0308933	0.0252280
	0.0000257	0.9994070	0.0000033			
	0.0497502	0.0000181	0.9988914			
L	0.9996580	0.0000015	0.0545503	0.0009255	0.0307683	0.0251279
	0.0003653	0.9990864	0.0000083			
	0.0520015	0.0003210	0.9987280			

Statistic For All Samples	**Mean of MAC:**			**Peak Error Norm of MAC Matrix:**	
	0.9996532	0.0003015	0.0585217	Diagonal Terms	0.0015762
	0.0002295	0.9992771	0.0003152	Off-Diagonal Terms	0.0351383
	0.0518500	0.0008179	0.9986334	Over-all Terms	0.0286918

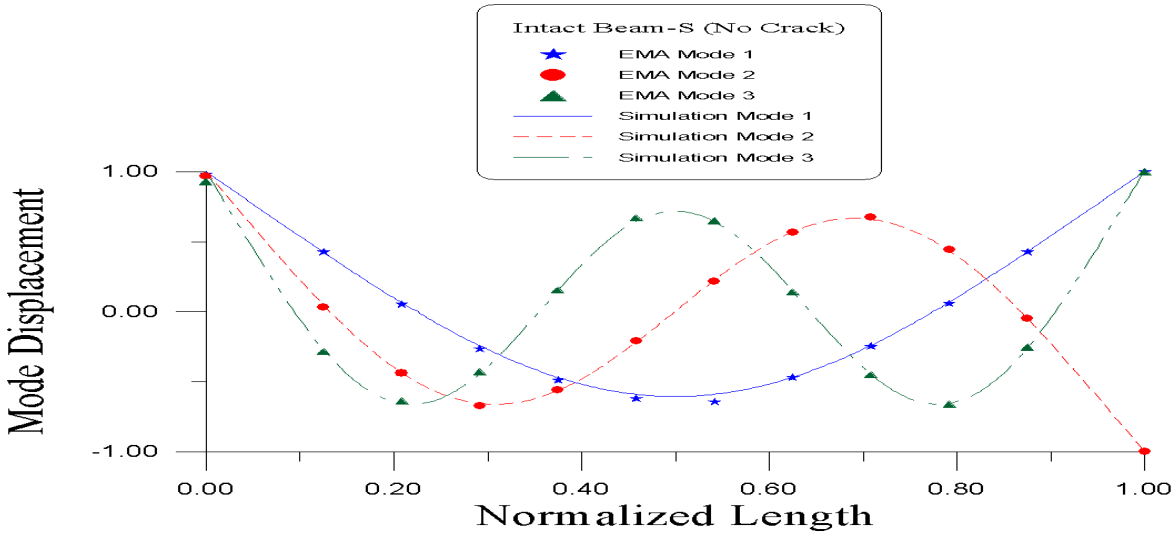

(a) Beam-S

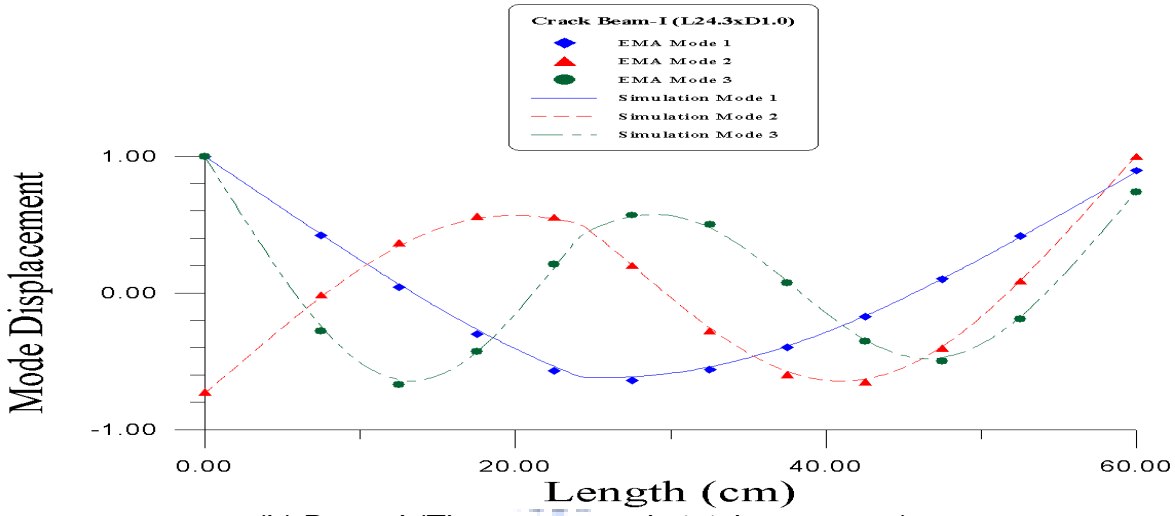

(b) Beam-I (The worse one in total error norm)

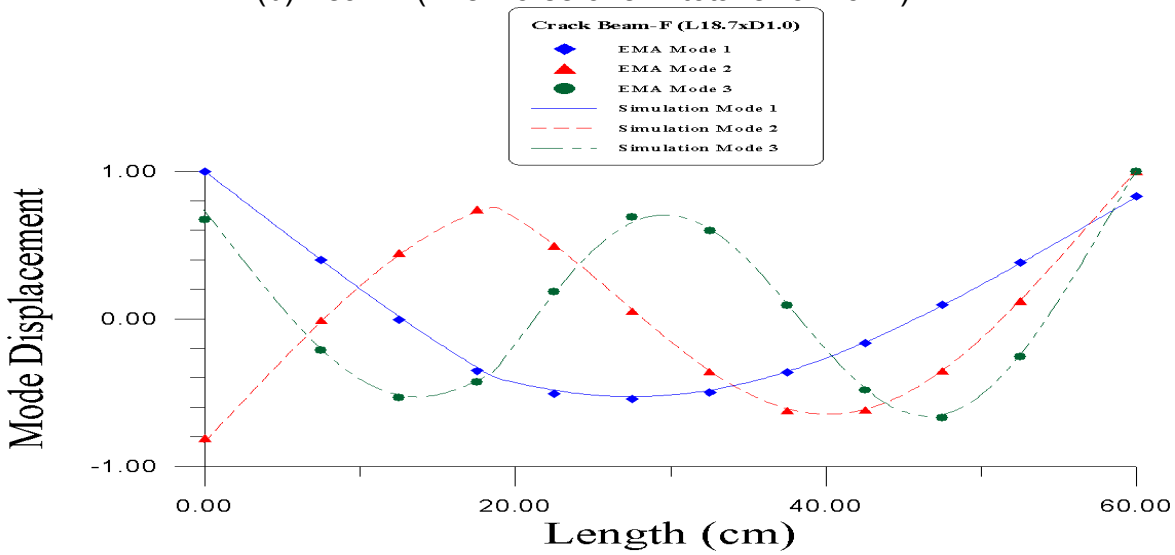

(c) Beam-F (The best one in total error norm)

Figure 11. Mode shape comparison between simulation & EMA

CHAPTER 4
Dynamic Characteristics of Cracked Beam and the Damage Identification Process

In physical sense, the crack existence in structure system will reduce its stiffness when compared with it in intact state. Its natural frequencies will be reduced; the mode shapes and curvature mode shapes will be also changed. When system mass density or Young's modulus of the entirely structure are varied for certain reason, its frequencies will also changed, but there will be not affect on the mode shapes and curvature mode shapes.

In this study, by selecting appropriate features from vibration responses, we can detect the damage location and then identify its severity. The simulation and experimental results shown in the following sessions are supported for these conclusions.

4.1 Definition of the LDI Index

The previous researchers, Pandey et al. [21] introduced the application of curvature mode shape for the detection of damage location. In this research, we authors defined an index for crack location detection, named as LDI (Location Detect Index). For Euler-Bernoulli beam, the strain energy(Ui) of an intact beam with respect to mode shape-i (ϕ_i) can be expressed as:

$$U_i = \frac{1}{2}\int_0^l EI\left(\frac{\partial^2 \phi_i(x)}{\partial x^2}\right)^2 dx \qquad (4.1)$$

where EI, l were the section rigidity and the length of beam. For an infinitesimal length dx located at xj along beam's axis, the strain energy of length dx can be expressed by u_{ij},

$$u_{ij} = \frac{1}{2} EI\left(x_j\right)\left(\frac{\partial^2 \phi_i\left(x_j\right)}{\partial x^2}\right)^2 dx \tag{4.2}$$

The authors defined the energy fraction with respect to total energy of entire beam U_i as F_{ij},

$$F_{ij} = u_{ij} / U_i \tag{4.3}$$

$$\int_0^l F_{ij} = 1.0 \tag{4.4}$$

For the same operation, for a cracked beam, we have：

$$U_i^* = \frac{1}{2}\int_0^l EI\left(\frac{\partial^2 \phi_i^*\left(x\right)}{\partial x^2}\right)^2 dx \tag{4.5}$$

$$u_{ij}^* = \frac{1}{2} EI\left(x_j\right)\left(\frac{\partial^2 \phi_i^*\left(x_j\right)}{\partial x^2}\right)^2 dx \tag{4.6}$$

$$F_{ij}^* = u_{ij}^* / U_i^* \tag{4.7}$$

$$\int_0^l F_{ij}^* = 1.0 \tag{4.8}$$

where U_i^*, u_{ij}^*, ψ_i^* and F_{ij}^* are strain energy, strain energy of infinitesimal length dx, mode shape-i and energy fraction of cracked beam respectively.

Let $\delta\kappa_{ij}$ as the temporary feature for location detection and it can be expressed as follows：

$$\delta\kappa_{ij} = F_{ij}^* - F_{ij} \tag{4.9}$$

by the normalization operation, we have the location's discrimination feature LDI as follows：

$$LDI\left(x_j\right) = \delta\kappa_{ij} \Big/ \{\frac{1}{2} EI\left(x_j\right) dx\} = \left(\frac{\partial^2 \phi_i^*\left(x_j\right)}{\partial x^2}\right)^2 \Big/ U_i^* - \left(\frac{\partial^2 \phi_i\left(x_j\right)}{\partial x^2}\right)^2 \Big/ U_i \tag{4.10}$$

The authors calculate each of the discrete point of the curvature related feature by central difference and then plot it along beam axis to complete the LDI curve.

For sample beam G, H, and I, all its crack location happened at 24.3mm but with different crack depths, 0.6cm, 0.8cm and 1.0cm, by examining the LDI index on the simulation result regarding mode 1, 2 and 3 shown in Fig. 12(a), (b) and (c) and EMA result for mode 1, 2 and 3 in Fig. 13(a), (b) and (c). We found the LDI index works well and it is consistent between simulation and EMA reach the below conclusions:

(1) Only at the location of crack will caused significant change on LDI by a sharp peak.
(2) The deeper crack depth will made the peak of LDI curve sharper.
(3) In practical EMA, due to limited impact location (sensors) applied, the LDI index will lose its accuracy to indicate the crack location due to larger measurement spacing, there will be discussion in session 5.4. (Refer to Fig. 13(c) mode 3 of EMA)
(4) In practical EMA, the authors also found that the intensity of LDI is stronger in low mode, in beam-I case almost double amplitude for mode 1 and 2 (Refer to Fig. 13(a) and (b) of EMA)
(5) There will no curvature change when crack located on the anti-node of modal curvature.

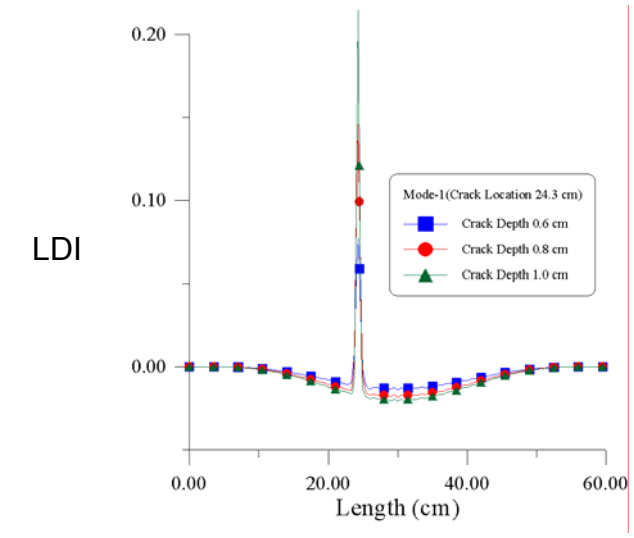

(a) Mode 1

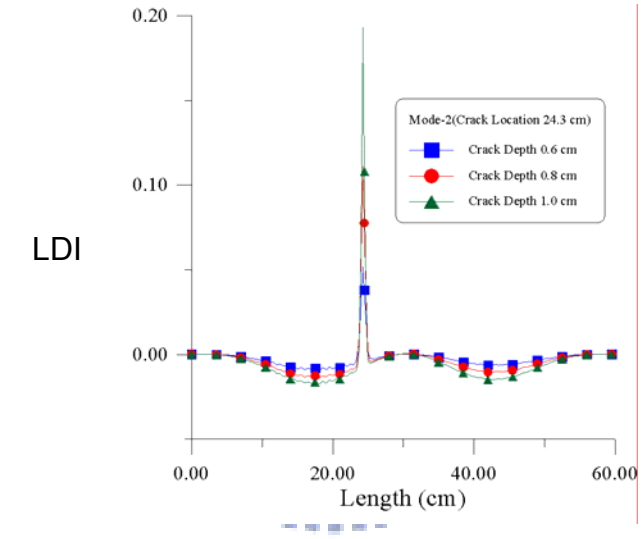

(b) Mode 2

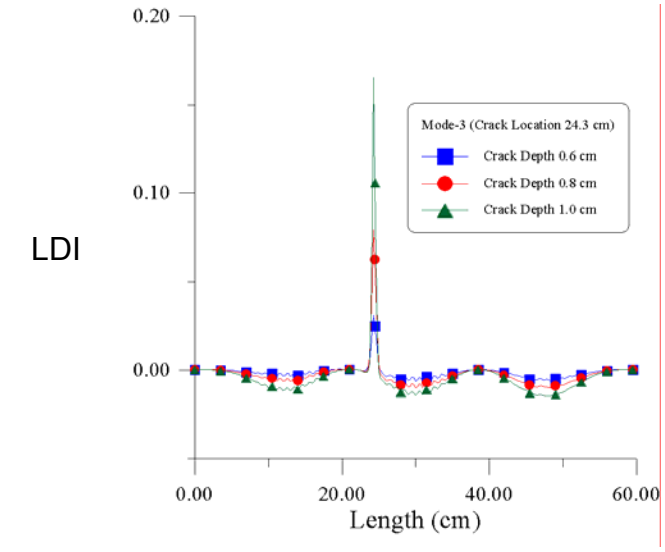

(c) Mode 3

Figure 12 LDI index by simulation (Beam G, H, & I, crack located on 24.3mm)

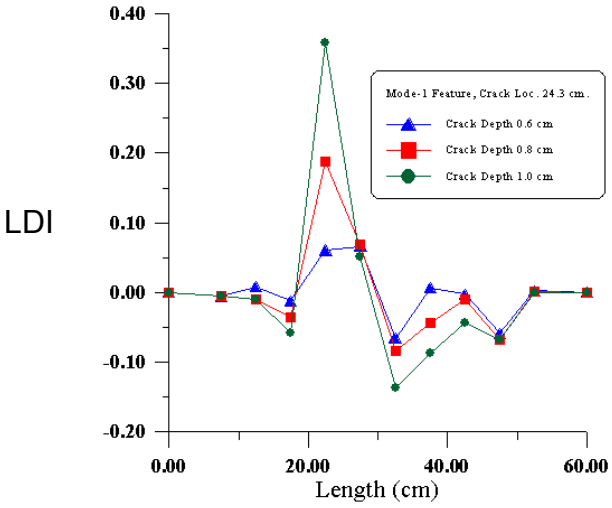

(a) mode-1

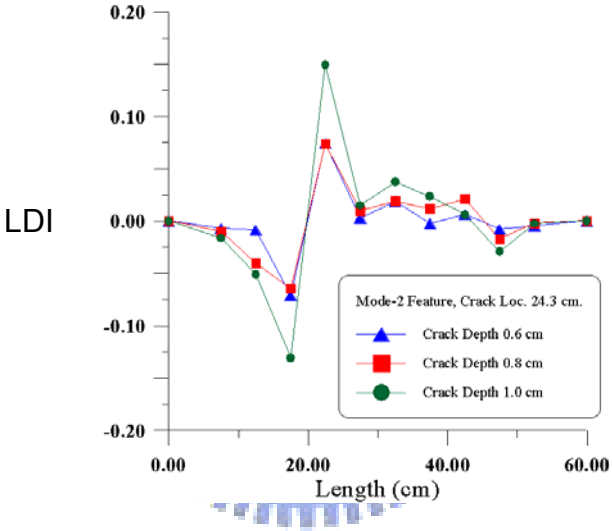

(b) mode-2

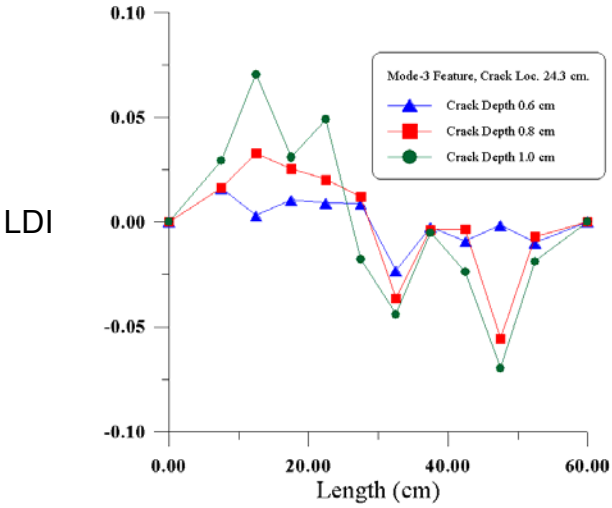

(c) mode-3

Figure 13. LDI index by EMA (Beam G, H, & I)

4.2 Definition of FCI curve

Modal frequency will changed due to crack existence on specific location and depth. Refer to Fig. 14, the EMA result is represented by point symbols, and line symbols are for simulation result for comparison purpose. The line, also called FCI (Frequency Change Index) curve, from simulation was made by a frequency change due to a constant crack depth with different crack location which is traveling along beam length.

The observation from Fig. 14 can be concluded as following:

(1) The crack will made modal frequency changed, we observed that the deeper crack depth made the larger amplitude on FCI curve

(2) The FCI curve from frequency change is in accordance with modal curvature shape, there will no frequency change on the anti-node of modal curvature shape

(3) The frequency change possesses symmetry property among spatial distribution, so we need to find crack location before identify its severity to avoid finding the fault crack location on the symmetry side.

(4) By judging from the changes of each modal frequency and set 2% tolerance limit in general engineering, the authors defined it is a shallow crack beam with the crack depth is least than 1/4 of depth. A sample beam (beam-N) in session 5.5 is designed to test for the effectiveness of proposed method.

The specific point on each FCI curve represents a damage state (certain crack depth and location) of cracked beam. The FCI index is a significant feature for finding crack severity. The authors then defined the frequency change as a specific point on FCI curve. It can be expressed as:

$$FCI(\Delta f_{j,damaged}) = \frac{f_{j,\mathrm{int}act} - f_{j,damaged}}{f_{j,\mathrm{int}act}} * 100(\%) \qquad (4.11)$$

where $f_{j,\mathrm{int}act}$ and $f_{j,damaged}$ are the frequency of mode-*j* for intact and damaged beam respectively.

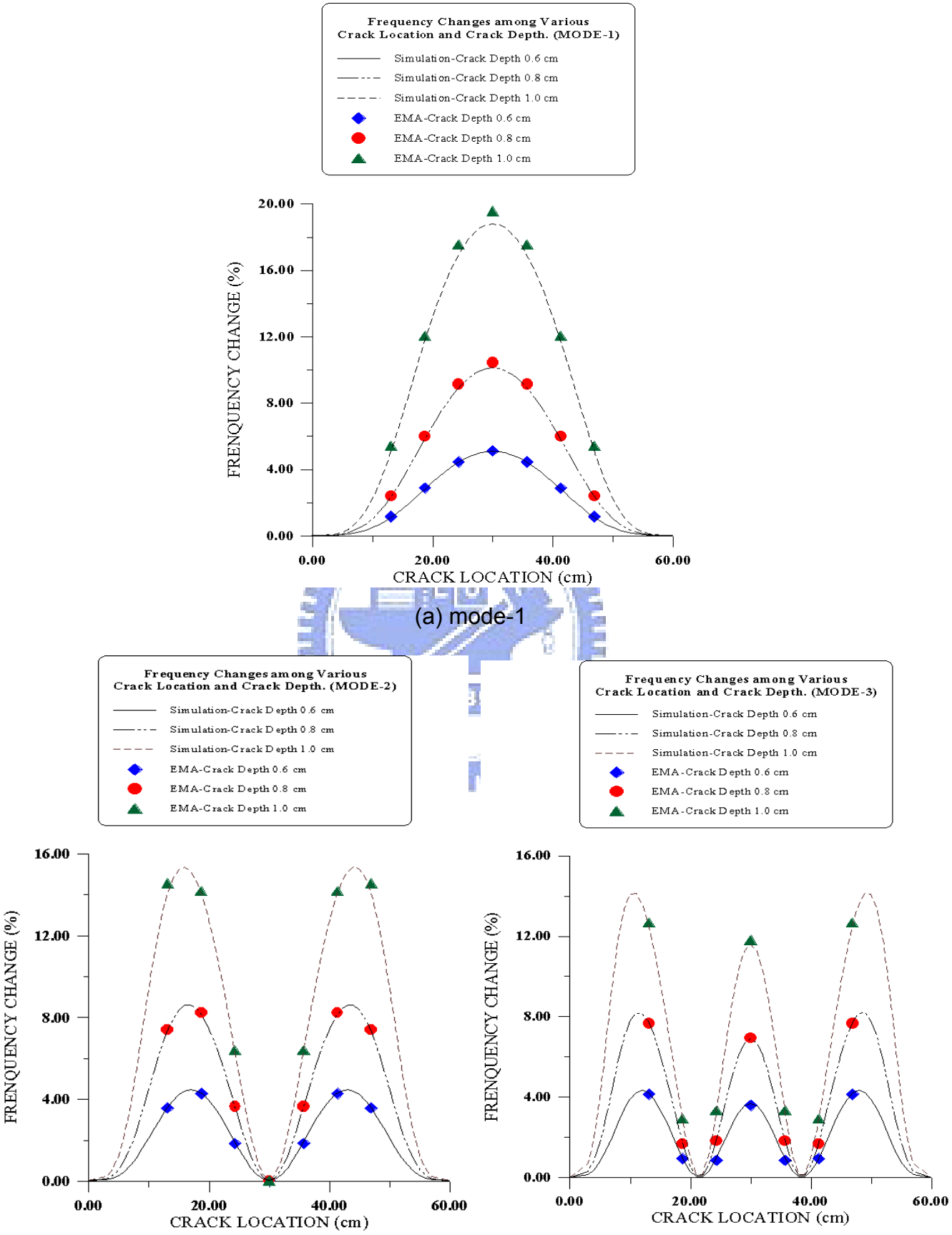

Figure 14. Frequency change due to crack existence by simulation & EMA

4.3 FCI for Depth Identification of Single Crack Beam for Property Invariant System with Noise-free Measurement

When we have the noise-free measured frequency from EMA for a property invariant structure system, the table lookup process was adopted for damage severity estimation. After the crack location identified by LDI index, we can identify the unknown crack depth by applying linear interpolation between two FCI curves. These FCI curves were above and below the EMA's on the specific crack location from simulation database. The authors increase the resolution of database to 1/16 of beam depth to avoid the calculation complexity, a linear interpolating then can be applied for unknown crack depth (β_x) was shown as below and illustrated by Fig. 15.

$$\beta_x = \beta_l + \frac{\Delta f_x - \Delta f_l}{\Delta f_u - \Delta f_l} * (\beta_u - \beta_l) \tag{4.12}$$

where Δf_x was calculated by Eq. (4.11) from the EMA measured frequencies (f_x) for unknown damage state, Δf_u and Δf_l were points on FCI curves that were also calculated by Eq. (4.11) on the above frequency(f_u) and below frequency(f_l) compared with the EMA measured frequencies(f_x), β_u and β_l were crack depths with respect to Δf_u and Δf_l accordingly. By inserting Eq. (4.11) into Eq. (4.12), we also have Eq. (4.13) as follows:

$$\beta_x = \beta_l + \frac{f_x - f_l}{f_u - f_l} * (\beta_u - \beta_l) \tag{4.13}$$

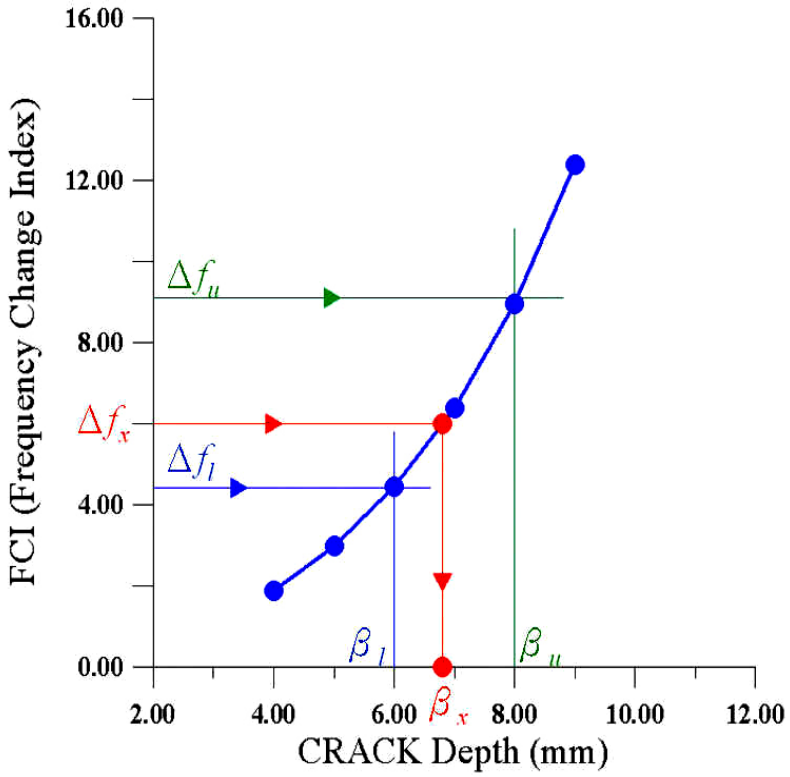

Figure 15. Crack depth assessment for property invariant beam structure

4.4 Influences of the Variation of Stiffness and Mass Density on LDI and FCI index

In order to clarify the effect of material property variation on LDI and FCI index, the authors prepared a simulated cracked beam (Beam-I, crack located 243mm, depth 10 mm) with a series combinations of different levels of mass density and Young's modulus variance that ranged from ±80% to ±120% of their mean value [15] [16]. It should emphasize that hear mentioned the stiffness variation is comes from environmental factor and other than the stiffness reduction due to the crack existence.

To review the result of Fig. 16, we can conclude that due to the stiffness and mass variation affecting the structure in a uniform way for the entire beam structure, the mode shape changed insignificantly on the variations, and the algorithm for crack location identification was held for the property variant systems. The LDI index can still indicate clearly for the crack location among various variation scenarios. The LDI index works well and robust for systems with uniform material property variations.

From the observation of Fig. 17, we found that the FCI index changed approximately ±20% when compared to invariant system. Hence, we should take into account the influences of property variations when applying FCI index for severity assessment. In the research, the authors represent these effects by statistical FCI databases, which were generated by LHS sampling in Monte Carlo simulation on beam with certain damage states incorporated with different level variances of mass density and Young's modulus.

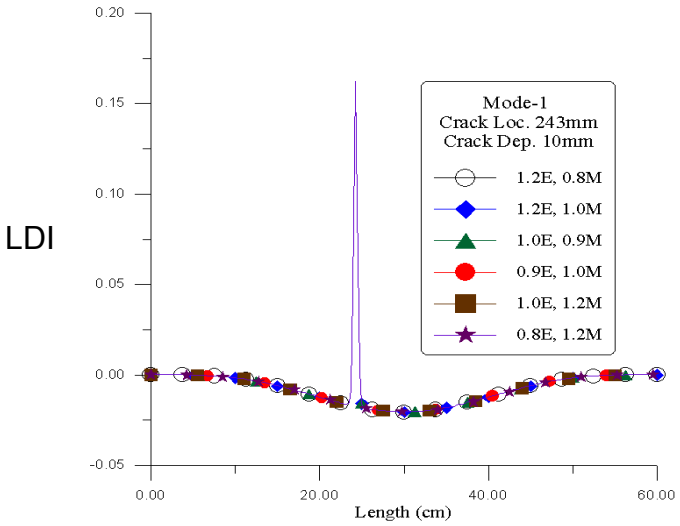

(a) mode-1

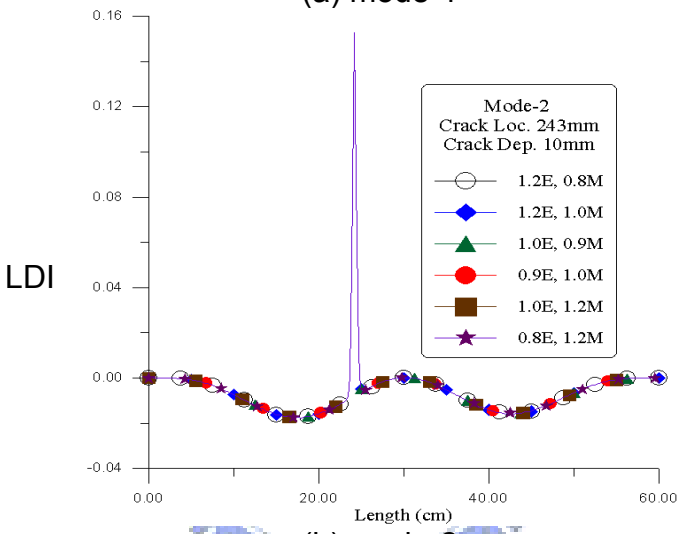

(b) mode-2

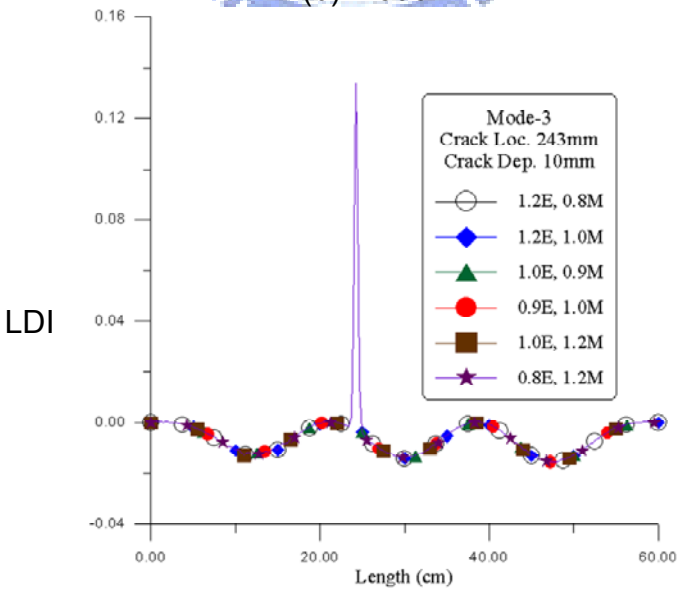

(c) mode-3

Figure 16. LDI index curve for property varied system (Beam-I, by simulation)

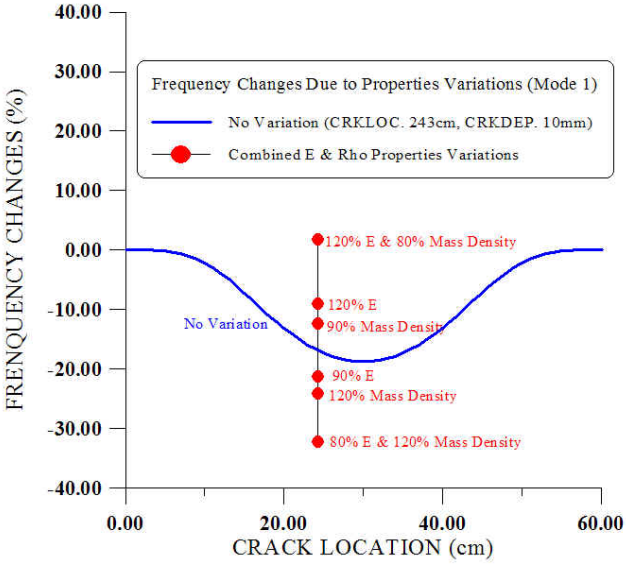

(a) mode-1

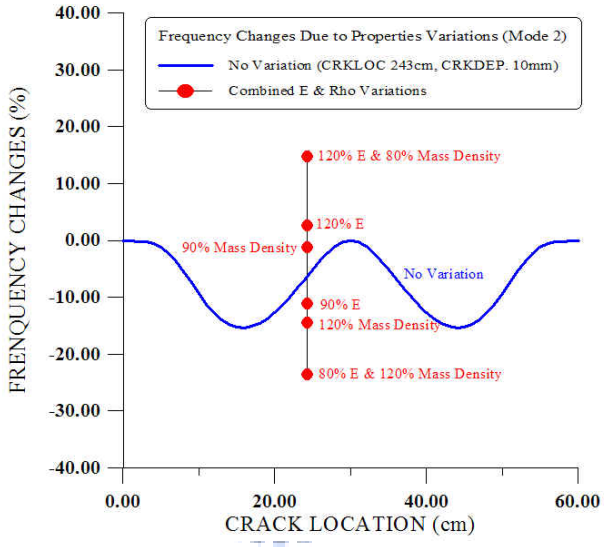

(b) mode-2

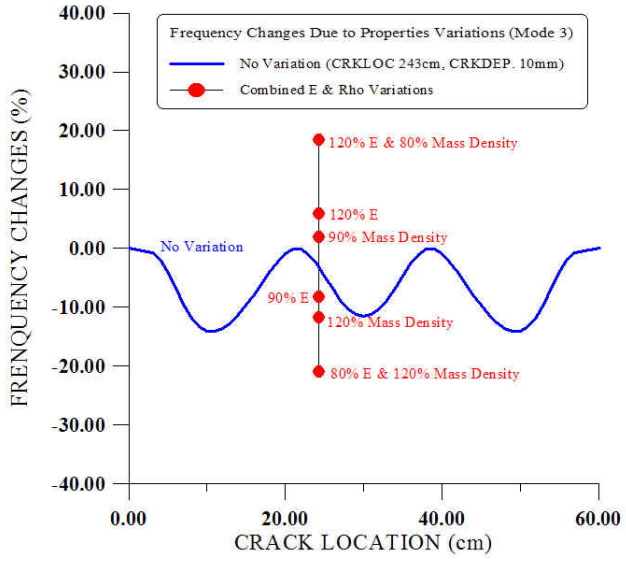

(b) mode-3

Figure 17. FCI index due to property variations (Beam-I, by simulation)

4.5 FCI for Depth Identification of Multiple Cracks Beam for Property Invariant System with Noise-free Measurement

The LDI index curve can be applied to multiple cracks case directly. However, with compared to single crack case, the authors should do a little modification for depth identification of multiple cracks case due to the frequencies change were affected by all of the cracks in the beam.

When we have the crack locations from LDI index curve, we should extend the single crack FCI curve shown in Fig. 15 to build up a set of FCI contour curve as shown in Fig. 18 which was based on known crack locations, and each of the contour curve from specific normal mode represented the frequency change due to multiple cracks' existence. To overlap these two contour curves and then the crack depths were identified by the intersection as shown in Fig. 19. A 2-crack beam example will be discussed in session 5.6 for demonstration.

We should noticed that when the crack number is more than two, its crack location can be assessed by the same LDI process, for the FCI database, we need to apply suitable mathematical tool to determine all the depths simultaneously. The artificial neural network could be an effective tool to achieve this purpose and need further study in advance, it will contain the training sample preparation, the sample training process and then used as the reference database for multiple crack depth assessment.

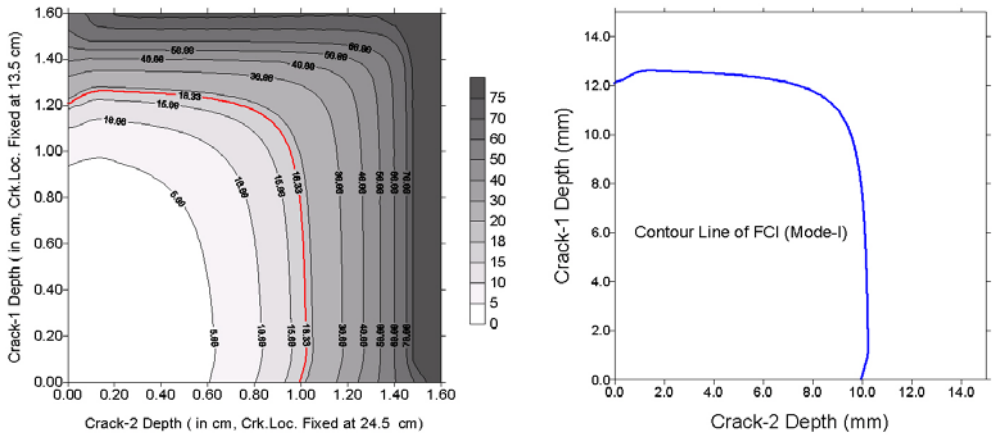

(a) Contour Line of Mode I

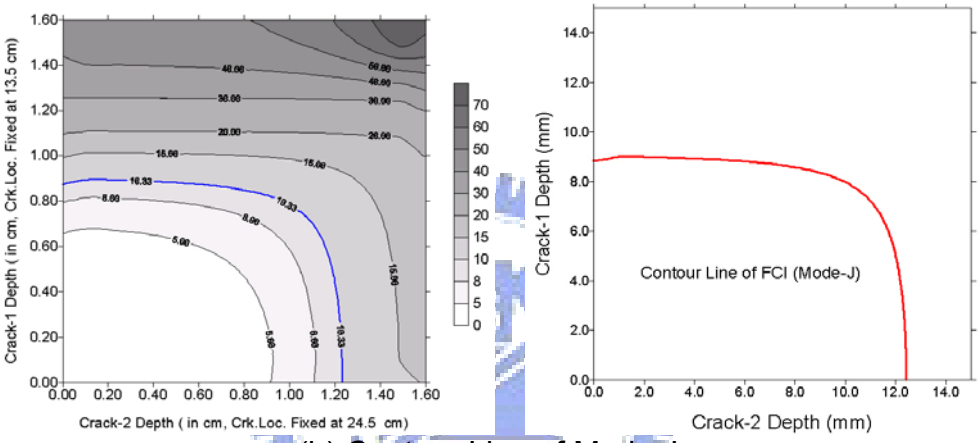

(b) Contour Line of Mode J

Figure 18. FCI Contour Lines due to multiple cracks existence

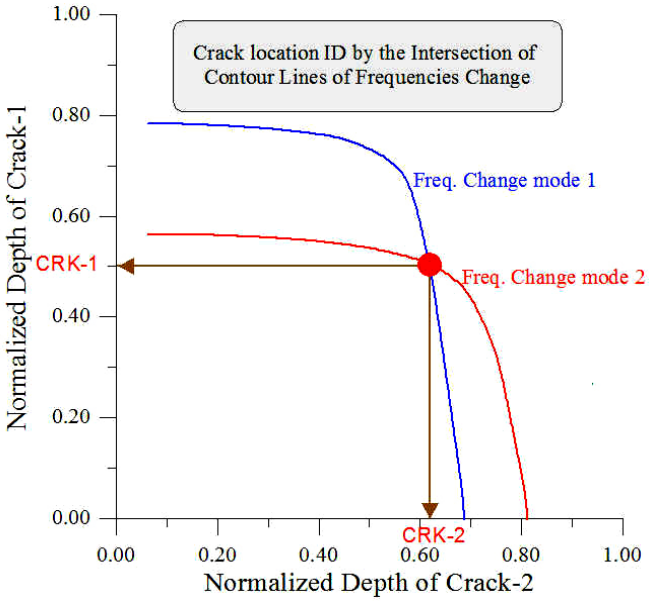

Figure.19. Determination of Crack Depths by the Intersection of Two FCI Contour Lines

4.6 Estimation of Crack Depth Probability for Variant Systems with Noised Measure Frequency

The severity identification process discussed in session 4.2, 4.3 and 4.5 were for the property invariant structure system and noise-free measured modal frequency. When the system mass density and stiffness were varied, the FCI simulation databases need to be extended. Basically, in the invariant system, for specific damage state of structure, its frequency change was a certain value only, it will map to a certain and confirmed point on FCI curve as shown in Fig. 15 or Fig. 19. But for a property variant system, for a specific damage state, the property variations will cause the change of frequency varied, then the corresponding point on FCI curve will be "smeared" as shown in Fig. 20. Usually we use a distribution function to describe the smearing phenomenon, for example, by the Gaussian distribution, and the noise polluted measured modal frequency could also described in a Gaussian distribution manner as shown in Fig. 21.

Since the FCI curve possesses a probability distribution characteristic in variant system, the results of identification will also display in a presence of probability distribution. As shown in Fig. 20 and 21, in statistical damage database, every point on FCI curve was accompanied with a Gaussian distribution, when we applied the measured frequency by EMA in probability distribution to find the unknown crack depths, we found that the probability distribution with mean value f_x was overlapped with several Gaussian distribution curves which represented for different damage states (crack depth). Each of overlapping represented the probability on these damage states. Hence, for a single noise polluted measured frequency by EMA, we will have several possible crack depths with its probability. By collecting all the probabilities along various crack depths, the identified results will present by a probability distribution curve.

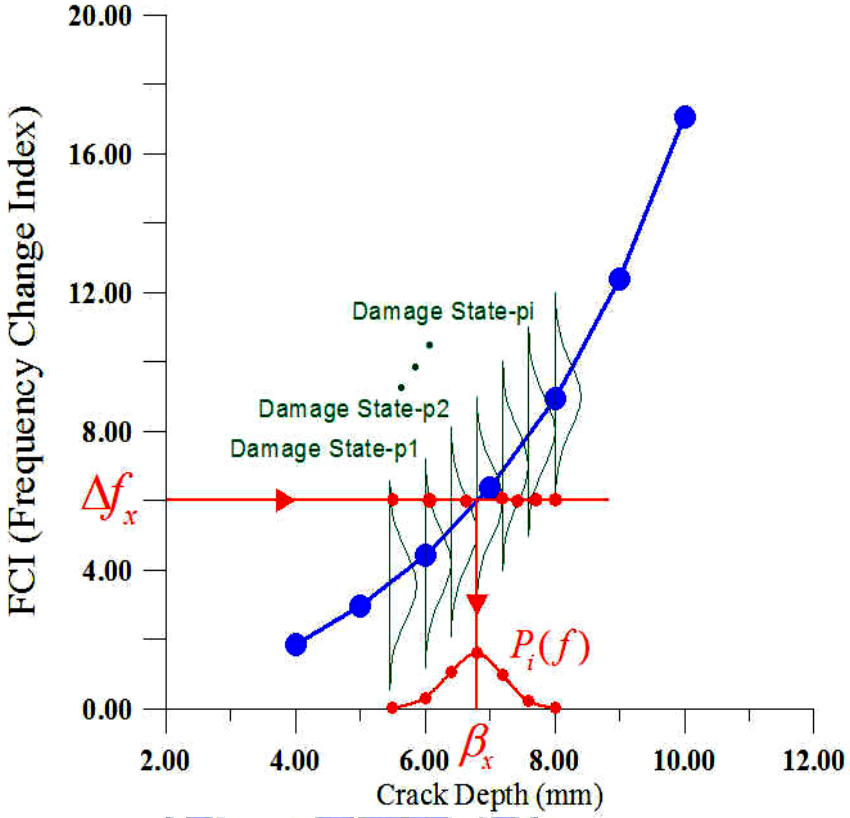

Figure 20. Crack Depth Assessment for Property Variant System

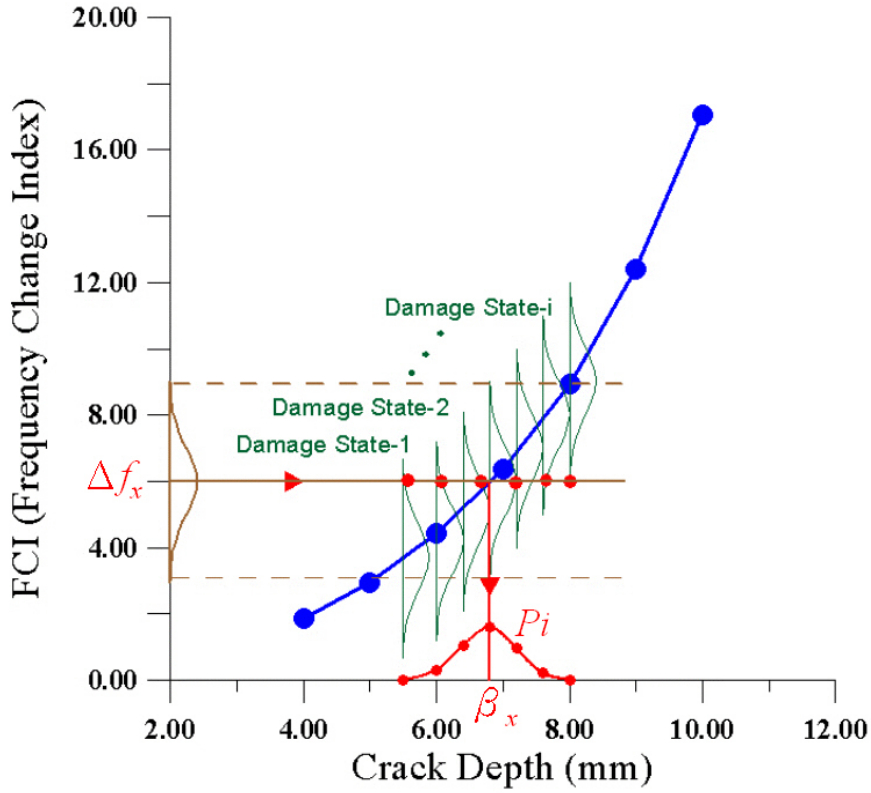

Figure 21. Crack Depth Assessment for Property Variant System subjected to noised measurement

Due to the measured frequency was noise polluted that we may represent the measured modal frequency by a probability distribution function. Assume that the material property variation was independent with measurement noise. Each probability (*Pi)* for damage state-*i* (crack depth) can be calculated by the following equation:

$$P_i = \int_{fa}^{fb} p_i(f) \text{ x } p^{EMA}(f_x)\, df \tag{4.14}$$

where f_x was calculated by the mean of measured frequency, and $p_i(f)$ was the probability distribution function of modal frequency in simulation database for damage state-*i* (crack depth), and the $p^{EMA}(f_x)$ was the probability distribution function of measured frequency with noise, the upper bound and lower bound frequency *fb*, *fa* should be determined by confidence level and the statistical t-test [12] that we should discuss later in this session. Both of the $p_i(f)$ and $p^{EMA}(f_x)$ were defined by the Gaussian distribution function *G(f)* as below.

$$G(f) = \frac{1}{\sigma\sqrt{2\pi}} \exp[-\frac{1}{2}(\frac{f-\mu}{\sigma})^2] \tag{4.15}$$

The statistical t-test was used to assess statistical significance of damage-sensitive features of EMA with the data in the simulated damage database. As stated above in this session, the upper and lower bound frequency of probability function in Eq. (4.14) should be determined by confidence level and the statistical t-test. As described in reference [12], assigning 2 samples in population size n_1 and n_2 with sample mean $\overline{X_1}$ and $\overline{X_2}$ and standard deviation S_1 and S_2, a test statistic Z can be defined as Eq. (4.16) to describe the hypothesis $\overline{X_1} - \overline{X_2} = \alpha$,

$$Z = \frac{\overline{X_1} - \overline{X_2} - \alpha}{\sqrt{\frac{S_1^2}{n_1} + \frac{S_2^2}{n_2}}} \tag{4.16}$$

$$\left|\overline{X_1} - \overline{X_2}\right| \le 0 \tag{4.17}$$

Where n_1, n_2 should be large enough to invoke the central limit theory to satisfied the normal distribution assumption and α was an arbitrary constant and assumed to be 0.0 in this research. The authors then set up the hypothesis to test the statistical significance by Eq. (4.17) equation. By solving for Eq. (4.16), we can then state that there was approximately 99% confidence level of truth if $|Z| \leqq 3.0$.

After we have assigned the confidence level to 99%, the upper and lower bound frequency of Eq.(4.14) can be determined by measure the distance between the mean of EMA data and simulated database that should not exceed three times of root sum squared of the standard deviations of EMA data and from simulated database's.

We may notice that the all the discussion above adopted the figure in the single-crack case; however, the algorithm described was suitable both for multiple cracks and single crack example. Except that the statistical FCI was function of 1 crack depth for single crack, for the multiple cracks the statistical FCI was function of many depths on the specific locations identified.

4.7 Procedures for Crack Detection and Identification

Three major steps in the process flowchart in chapter 1 as shown in Fig. 1 and the procedures are described as follows.

4.7.1 Cracks Location Detection

When we had prepared the modal frequency and mode shape of damaged beam from EMA and the modal frequencies and mode shapes of intact beam from simulation, by analyzing the peak response of LDI, we can identify crack location by Eq.(4.10).

4.7.2 Generate Simulated Statistical FCI Database

Since we had obtained the crack locations of the damaged beam, to build up the damage severity database should be followed. For the property variant system, we need to describe the property variation in the form of mean and standard deviation of Gaussian distribution. By using the LHS sampling technique [15], we shall have a minimum but useful samples that incorporated with various E^*(stiffness variation), ρ^*(mass density variation) and ξ_i^*(specific crack depth). Where E^* and ρ^* were a specific variation value of stiffness and mass density randomly selected by LHS sampling, and the ξ_i^* denoted the specific depth of cracks from a series of possible cracks' depths. By assigning each set that composed of ξ_i^* with E^* and ρ^* for finite element normal mode analysis repeatedly, we could generate the simulated statistical FCI databases represented by its modal frequency and variation among various cracks' depths. The above process is also mentioned as the Monte Carlo simulation.

The same procedures were used for the property invariant system to generate simulated FCI database, except that for the deterministic system, there was no need to do Monte Carlo simulation due to the stiffness(E) and mass properties(ρ) that were all fixed with no variation. It required only doing the

deterministic normal mode analysis for one set of specific cracks' depth(ξ_i^*) among the possible cracks' depths to build the database.

4.7.3 Identify Cracks Depth

For the variant system, by assigning confidence level to approximate 99%, then the statistical significance of damage level was examined by t-test, the upper and lower bound of integration in Eq. (4.14) then determined. Since we have built the simulated statistical FCI databases for property variant system, we can map the noised measured frequency by EMA to the data of simulated databases that were both represented in Gaussian distribution form, then the cracks' depth were assessed by its probability.

CHAPTER 5
Demonstration Examples

The damaged beam (Beam-I) was used to demonstrate the assessment of single crack beam with different measurement resolution. A single shallow depth cracked beam (Beam-N) was also used to test for the capability of the proposed method. Multiple cracks example was represented by a 2-crack beam (Beam-M), the assessment process was demonstrated as follows：

5.1 Crack Location Detect of Beam-I

From the finite element normal mode analysis and EMA data, we have the three lowest mode shapes of damaged beam and intact beam. The crack location can be detected by applying the LDI by Eq. (4.10) in session 3.1. By reviewing the results in Fig. 22(a), we found that the crack was located at 245mm by the peak of LDI index curve of mode 1 and 3; by mode 2 the crack was located at 235mm. When compared to the real crack location 243mm, the averaged absolute error was 1.64%.

5.2 Crack Depth Identification of Beam-I for Property Non-variant System

As discussed in chapter 4.7 and the procedures shown in Fig. 1, for a property non-variant system, we had built the simulated FCI database according to the crack location 245mm that was determined in the previous session. Then the unknown crack depth can be identified by Eq. (4.13). Since we had the EMA measured frequencies that were 193.43Hz, 602.38Hz and 1210.66Hz for the lowest three modes, by the interpolating process as shown in Fig. 23, we have crack depth 10.02mm, 10.26mm and 9.66mm for the three lowest modes respectively. The errors were +0.2%, +2.6% and –3.4% for the three modes and the averaged absolute error was 2.07%.

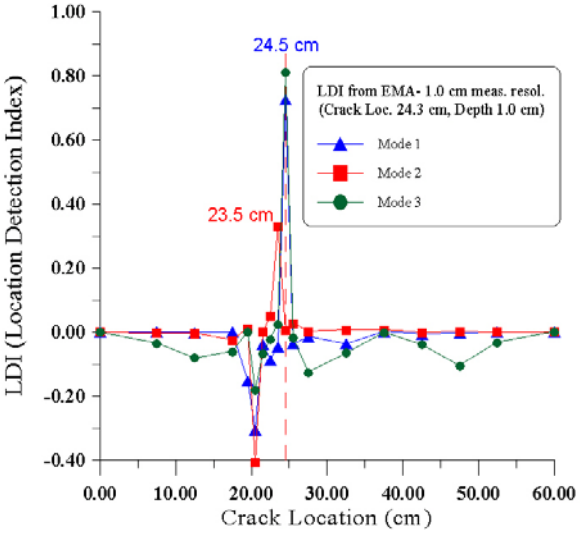

(a) Beam-I, Meas. Resol. 10mm

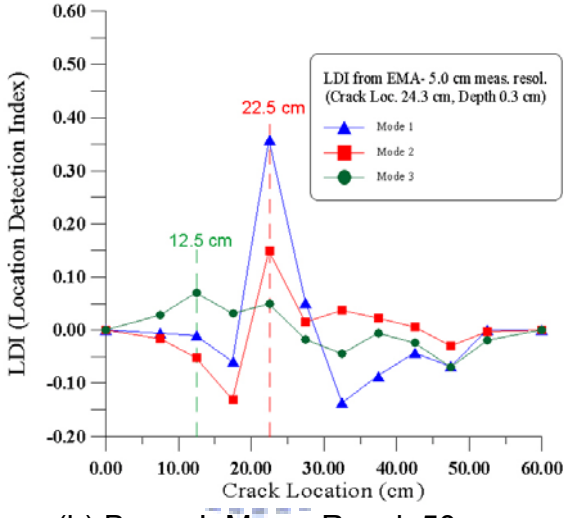

(b) Beam-I, Meas. Resol. 50mm

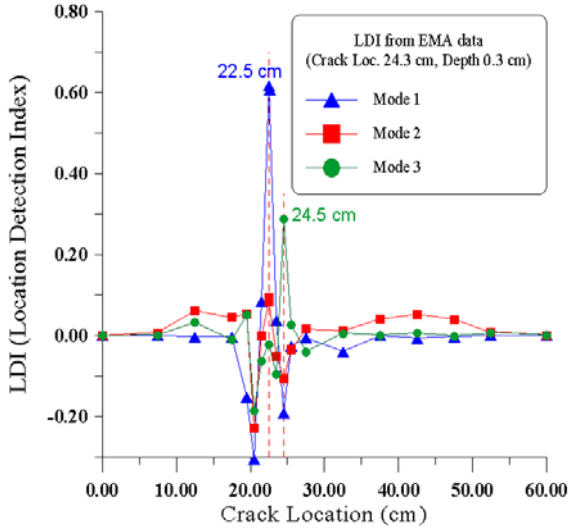

(c) Beam-N, Meas. Resol. 10mm

Figure 22. Crack location detect by LDI curve

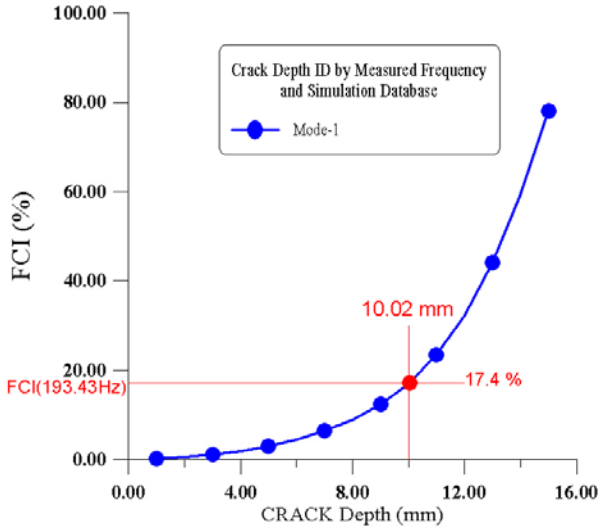

(a) Mode 1

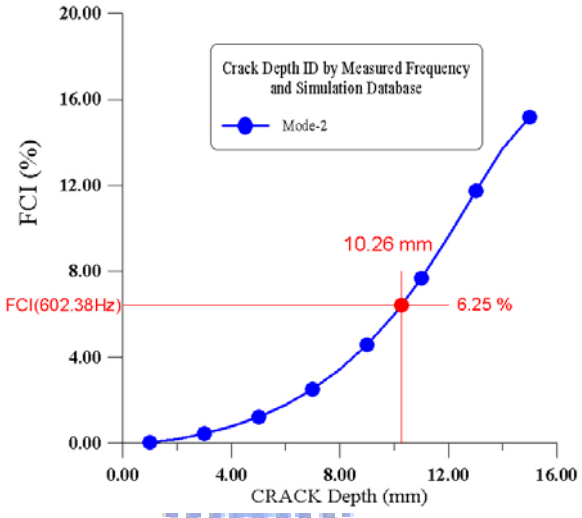

(b) Mode 2

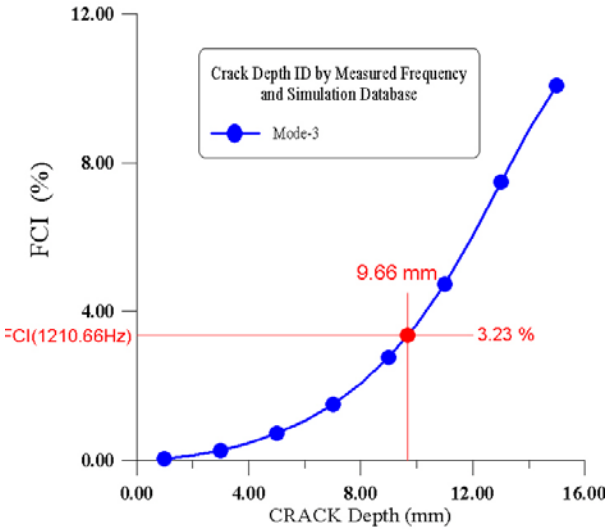

(c) Mode 3

Figure 23. Crack Depth Identification by FCI
(Beam-I, Meas. Resol. 10mm, Crk. Loc. 243mm, Depth 10mm)

5.3 Crack Depth Identification of Beam-I for Property Variant System

For a property variant system, refer to procedures described in session 4.7 and flowchart shown in Fig. 1, we need to build the simulated statistical FCI database according to the crack location found in session 5.1. In order to build the statistics database, we assumed the variations of mass density & Young's modulus were ±2%, ±5% and ±10% of its mean value. By sensitivity analysis, 300 samples were used for LHS sampling. The typical data from Monte Carlo simulation results on certain crack depth with different level of variations for different modes were shown in Table 4. Each set of mean with standard deviation represented a probability distribution on a point (crack depth) of statistical FCI curve as shown in Fig. 20 and 21.

Although the experiments controlled in the laboratory, there was still variability in the experimental data. For the study of noised measured frequency effects, the authors assumed that we have noise on the measured frequencies. The variations of noised frequency were assumed as ±2%, ±5% and ±10% of measured frequency incorporated with ±2%, ±5% and ±10% material variations. In Eq. (4.14) we could assess probability on specific severity by mapping the measured frequency to each of the probability distribution curves of statistical FCI database. By changing to different depths in sequence, we have probabilities at all depths.

The interpreted probability distributions of crack depth on material variations and varied noise level measured frequency were shown in Fig. 24. We have observed that from mode 1 results (1st row in Fig. 24), for 2% and 5% material variation, the maximum probability of crack depth all occurred at 10.0mm for 0%, 2%, 5% and 10% measured frequency noise, for 10% material variation, the maximum probability of crack depth occurred at 10.25mm for 0%, 2%, 5% and 10% noise in measured frequency. From mode 2 data (2nd row in Fig. 24), only results for 2% and 5% material variation with measured frequency noise least than 2% can be identified, the maximum probability of depth all occurred at 10.25mm. Results

from mode 3 (3rd row in Fig. 24), only the results of the material variation and noised measure frequency both least than 2% can be identified, the maximum probability of crack depth occurred at 9.75mm.

By reviewing Fig. 24 again, we found data in first mode; the crack depth has the distinct peak and the narrowest spreading on its probability distribution. This means that the lowest mode has less scattering on severity identification. We have also found that both the larger material variation and the larger noise level of measured frequency will made the probability distribution wider on severity and the reliability will be decreasing on the depths which had been identified.

Table 4. Monte Carlo Simulation Results among Various Crack Depth (Beam-I)

Depth of Crack (mm)	Variant Level of Mass Density & Young's Modulus (in % of mean)	Mode-1 (Hz)		Mode-2 (Hz)		Mode-3 (Hz)	
		Frequency	Standard Deviation	Frequency	Standard Deviation	Frequency	Standard Deviation
9.00	2 %	205.20	2.93	613.3	8.75	1217.0	17.35
	5 %	205.30	7.35	613.6	21.96	1217.0	43.57
	10 %	205.70	14.89	614.8	44.50	1220.0	88.29
9.50	2 %	200.10	2.85	609.0	8.69	1211.0	17.28
	5 %	200.30	7.17	609.3	21.81	1212.0	43.38
	10 %	200.60	14.52	610.5	44.19	1215.0	87.91
9.75	2 %	197.30	2.81	606.6	8.65	1209.0	17.24
	5 %	197.40	7.06	606.9	21.72	1209.0	43.28
	10 %	197.80	14.31	608.1	44.02	1212.0	87.70
10.00	2 %	194.30	2.77	604.2	8.62	1206.0	17.19
	5 %	194.40	6.96	604.6	21.64	1206.0	43.17
	10 %	194.80	14.10	605.7	43.85	1209.0	87.49
10.25	2 %	190.90	2.72	601.6	8.58	1202.0	17.15
	5 %	191.00	6.84	601.90	21.54	1203.0	43.06
	10 %	191.40	13.85	603.10	43.66	1205.0	87.25
10.50	2 %	187.30	2.67	598.9	8.54	1199.0	17.10
	5 %	187.40	6.71	599.3	21.45	1200.0	42.94
	10 %	187.80	13.59	600.4	43.46	1202.0	87.01
11.00	2 %	179.40	2.56	593.3	8.46	1192.0	17.00
	5 %	179.50	6.42	593.7	21.25	1193.0	42.68
	10 %	179.80	13.02	594.8	43.06	1195.0	86.50

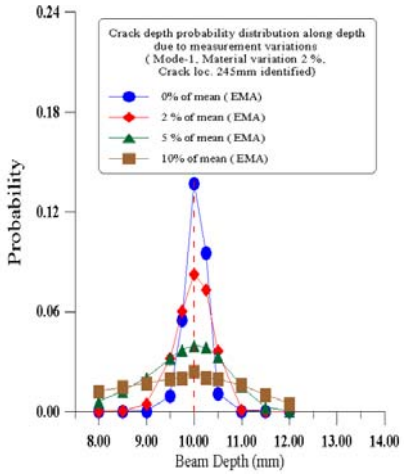

(a)2% material variation, mode 1

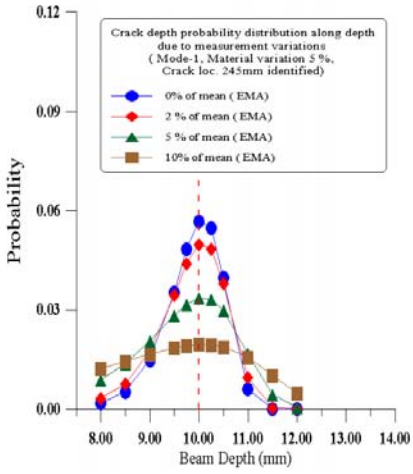

(b)5% material variation, mode 1

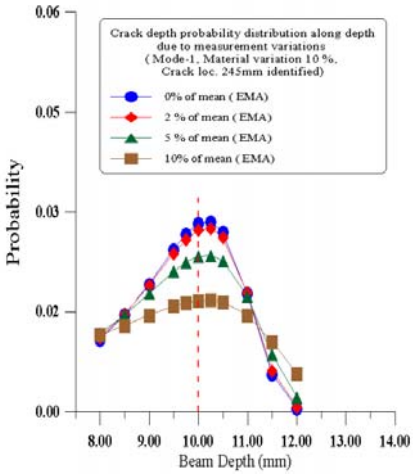

(c)10% material variation, mode 1

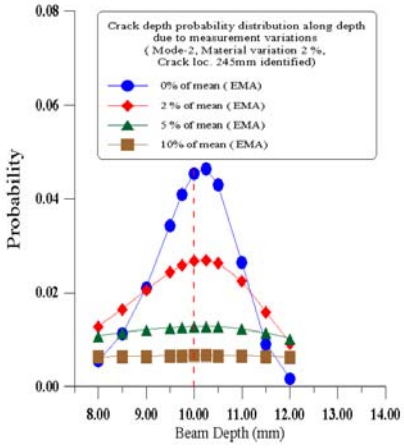

(d)2% material variation, mode 2

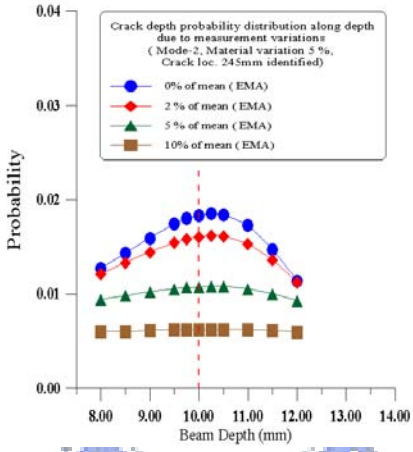

(e)5% material variation, mode 2

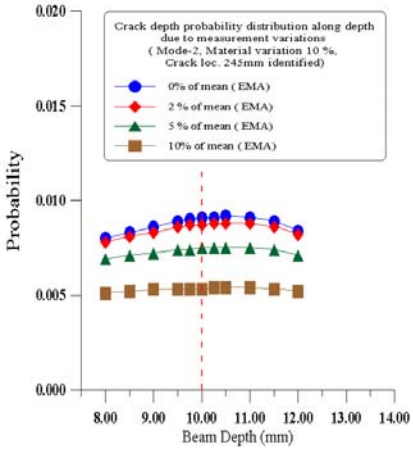

(f)10% material variation, mode 2

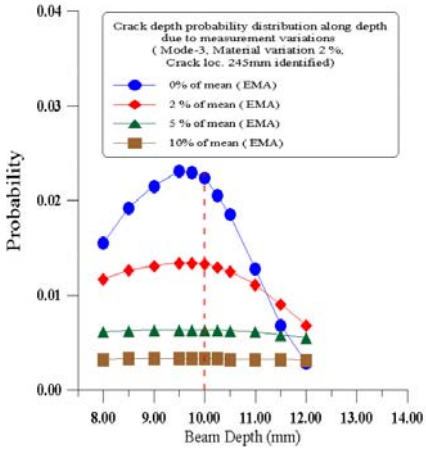

(i)2% material variation, mode 3

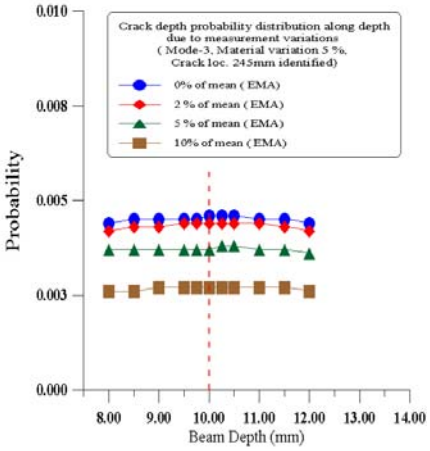

(j)5% material variation, mode 3

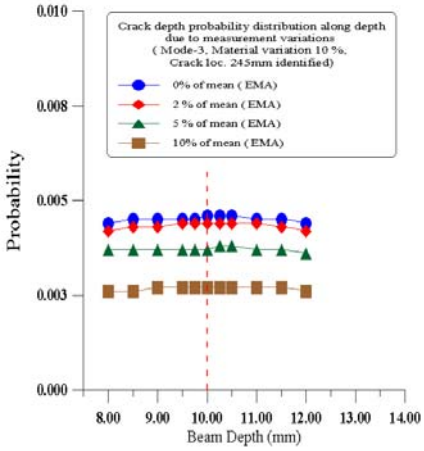

(k)10% material variation, mode 3

Figure 24. Probability distribution of Beam-I among varied crack depth (Meas. Resol. 10mm)

5.4 The Measurement Resolution Effects on Assessment Results

The above example was based on the assumption that we have the appropriate number of measurements; the authors took 10mm as the spacing between measurement points near the crack zone and 50mm~75mm on others, 18-impact locations in total. In this section, in order to test for the effectiveness of the proposed algorithm, the measurement spacing was extended to 50mm~75mm for the entire beam, 12-impact locations totally. According to the result of EMA and finite element normal mode analysis, the crack location can be detected as shown in Fig. 22(b). From the peak of LDI curve of mode 1 and 2 we found that the crack was located at 225 mm (-7.4% error). From mode 3 we have the crack located at 125 mm (-48.6% error). Mode 3 data lost its accuracy and it cannot be used for further identification on depth. With compared to the results of 18-impact measurement resolution (1.64% error), we have less accurate on crack location due to the larger measurement spacing.

For the property invariant system, took mode 1 and 2 results (crack location 225mm) as the basis to generate FCI database. With the same procedures described in the above example, by the interpolating process as shown in Fig. 25, the crack depth was identified by FCI, we have 10.26mm (+2.60% error), 8.50mm (-15.0% error) in crack depth for the first and second mode respectively. With compared to the results of above 18-impact measurement resolution example, its averaged absolute error of the lowest three modes (2.07%), we have less accurate results on crack location. Besides, due to the FCI database was based on crack location 225mm, the location was very closed to one of the node of curvature mode shape 3; hence we have poor result when applied mode 3 data for crack assessment.

For the property variant system with noised measurement, the statistical FCI database was also based on mode 1 and 2 results. For various property variation and different level measurement noise, the crack depth was determined by the

highest probability. The assessed probability distribution was shown in Fig. 26. From mode 1 results (1st row in Fig. 26), for 2%, 5%, 10% and material variation, the maximum probability of crack depth all occurred at 10.25mm for all level measurement noise. From mode 2 data (2nd row in Fig. 26), only results for 2% and 5% material variation with measurement noise least than 2% can be identified for crack depth, its maximum probability occurred at 8.50mm. Results from mode 3 (3rd row in Fig. 26), there was no clear indication for crack depth due to the crack location used for statistical FCI database was very closed to one of the node of curvature mode shape 3. With compared to the results of 18-impact measurement resolution example, 0.83% error for mode 1 and 2.5% error for mode 2 and 3, we have less accurate results on crack depth identified.

By reviewing Fig. 26 again, we have the same conclusion as the example of 18-impact measurement resolution that the result from first mode has the distinct peak and the narrowest spreading on its probability distribution on severity. The higher mode used in assessment, the larger material variation or the larger noise level of measured frequency will made the error larger, the probability lower and the distribution wider.

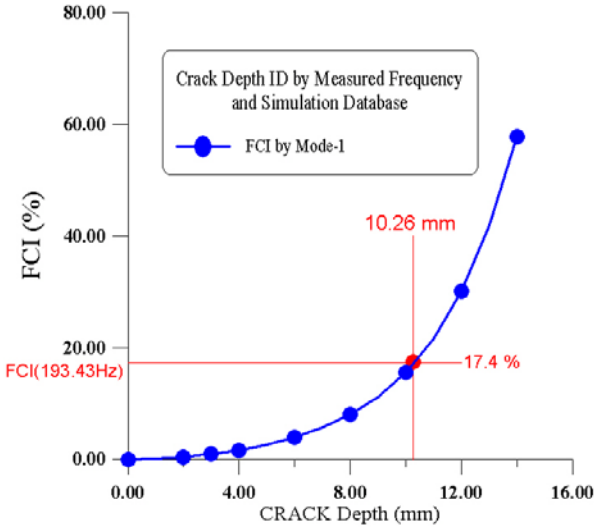

(a) Mode 1

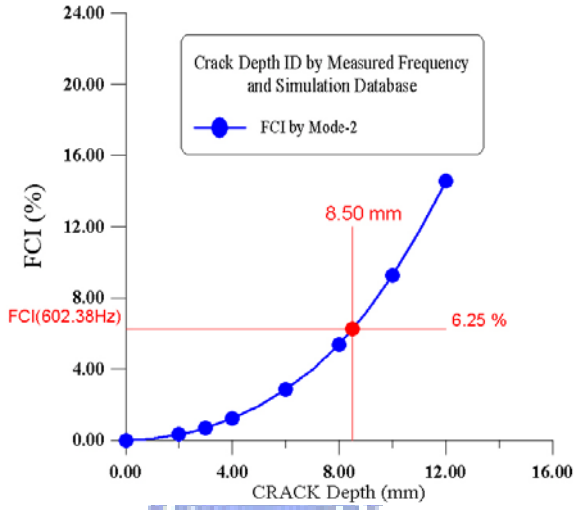

(b) Mode 2

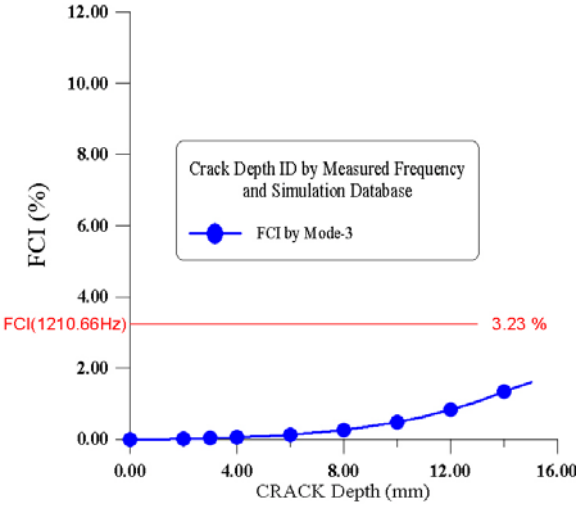

(c) Mode 3

Figure 25. Crack Depth Identification by FCI
(Beam-I, Meas. Resol. 50mm, Crk. Loc. 243mm, Depth 10mm)

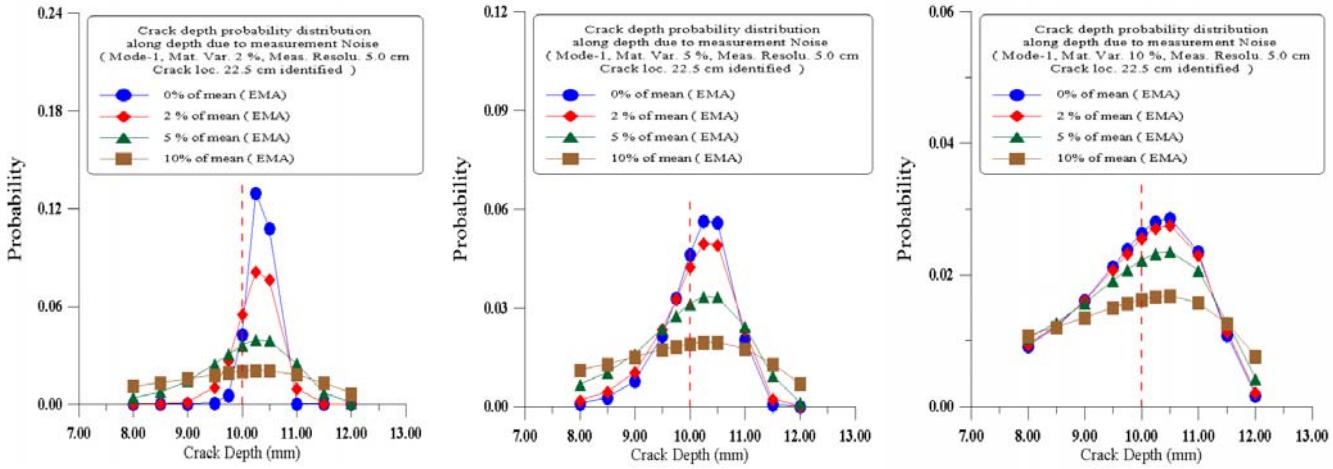

(a)2% material variation, mode 1

(b)5% material variation, mode 1

(c)10% material variation, mode 1

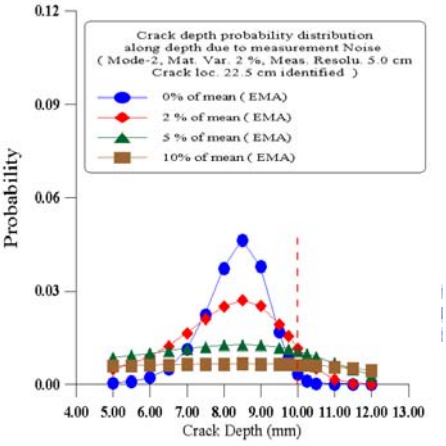

(d)2% material variation, mode 2

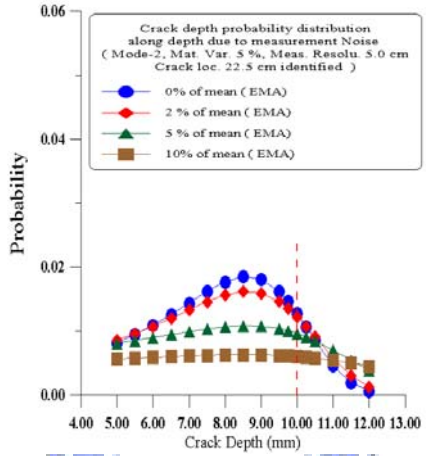

(e)5% material variation, mode 2

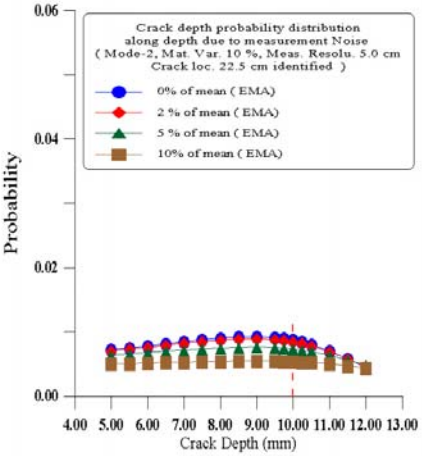

(f)10% material variation, mode 2

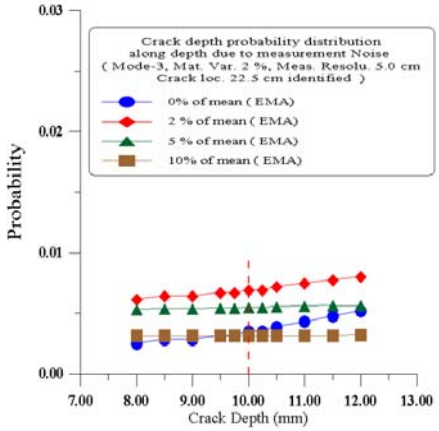

(i)2% material variation, mode 3

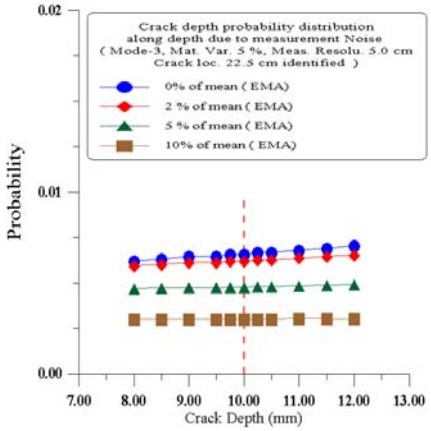

(j)5% material variation, mode 3

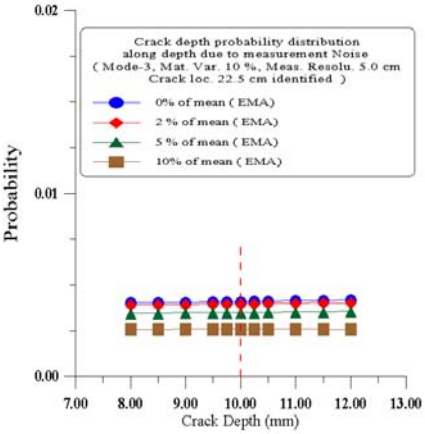

(k)10% material variation, mode 3

Figure 26. Probability distribution of Beam-I among varied crack depth (Meas. Resol. 50mm)

5.5 The Shallow Crack Depth Example (Beam-N Case)

It is always a challenge work to identify a small depth crack on structure. A sample beam, named as Beam-N, was designed to complete the study. For the convenient to compare with the Beam-I example, a cracked beam was manufactured by wire-cut with the same crack location 243mm but a smaller crack depth 3mm.

According to the finite element normal mode analysis result and EMA data (by 10 mm measurement resolution near the crack, 18-impact example), the crack location can be detected as shown in Fig. 22(c). From the peak of LDI curve of mode 1 and 2, we found that the crack was located at 225mm (-7.41% error) and from mode 3 we have the crack located at 245mm(+0.82% error). The averaged absolute error was 5.21%, with compared to the results of Beam-I we have larger error for a small crack depth beam example in crack location detection.

For the identification of shallow depth cracked beam in property invariant system, the authors took the average of mode 1 and 2 results (averaged crack location 232mm) as the basis to generate FCI database. With the same procedures as Beam-I, we had the EMA measured frequencies 231.78Hz, 639.68Hz and 1248.47Hz for the lowest three modes, by the interpolating process as shown in Fig. 27, the crack depth was identified by FCI as 3.09mm (+3.0% error), 2.60mm (-13.3% error), and 4.63mm(+54.3% error) for mode 1, 2 and mode 3 respectively, only mode 1 result was acceptable in accuracy. However, the small denominator (crack depth 3.0mm) made the large relative error. If we take a look at its absolute error, 0.09mm, 0.40mm, 1.63mm for mode 1, 2 and 3, with compared to the result of Beam-I, 0.02mm, 0.26 mm and 0.34mm; there were in the same error level except for mode 3. But, due to the large denominator (crack depth 10.0mm) we will have smaller absolute error for Beam-I.

For the crack depth identification of property variant system with noised frequency measured, the statistical FCI database was based on mode 1 and 2 results (crack location 232mm). The results of probability distribution assessed were shown in Fig. 28. We have observed that only the crack depth can be identified, by mode 1 under 2% material variations with no measurement noise, and the crack depth identified as 3.20mm (+6.67% error) by the highest probability. With compared to the results of Beam-I (10mm crack depth); its crack depth was 0.83% error for mode 1 and 2.5% error for mode 2 and 3, we have less accurate results on crack depth identified. We have found that first mode result of Beam-N do not have a sharp peak and a narrow spreading on its probability distribution. The probability distribution for mode 1 has the same shape as the higher mode with higher measurement noise in Fig 24 and 26.

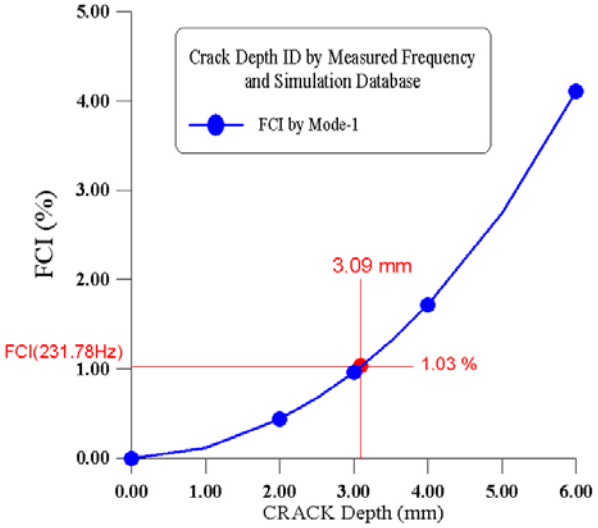

(a) Mode 1

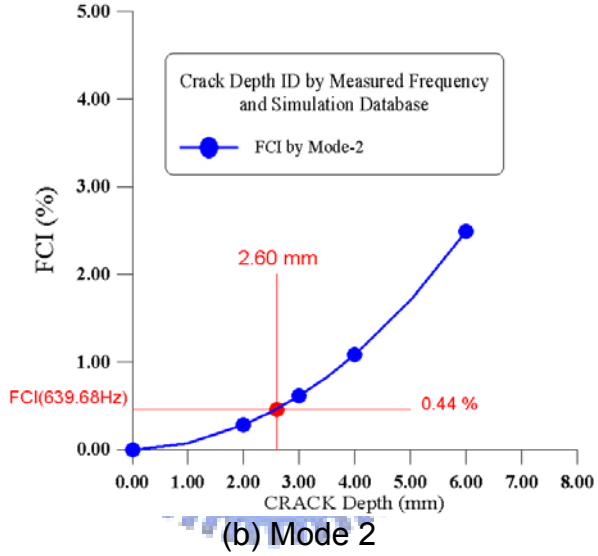

(b) Mode 2

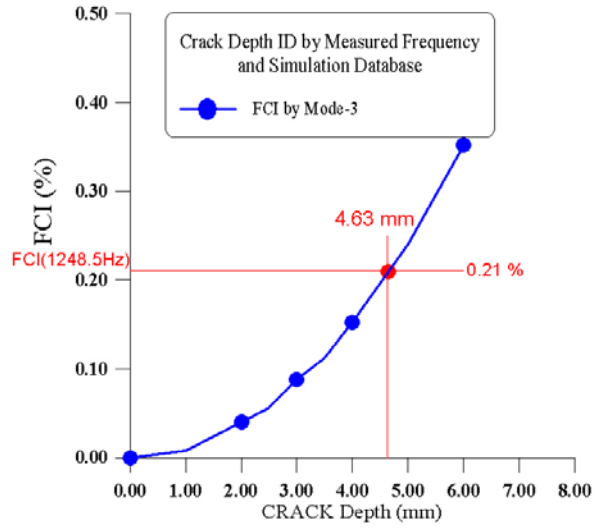

(c) Mode 3

Figure 27. Crack Depth Identification by FCI
(Beam-N, Meas. Resol. 10mm, Crk. Loc. 243 mm, Depth 3mm)

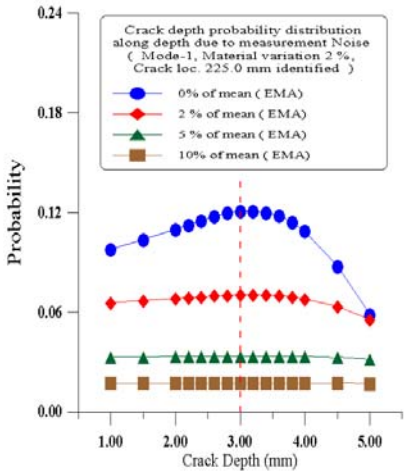

(a)2% material variation, mode 1

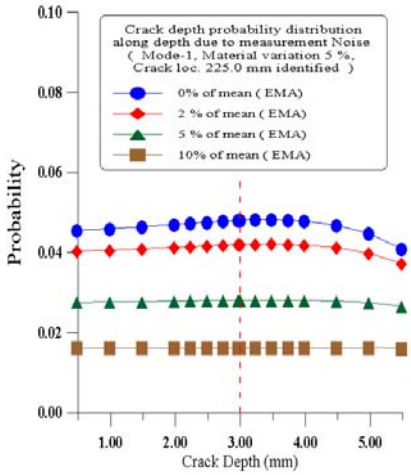

(b)5% material variation, mode 1

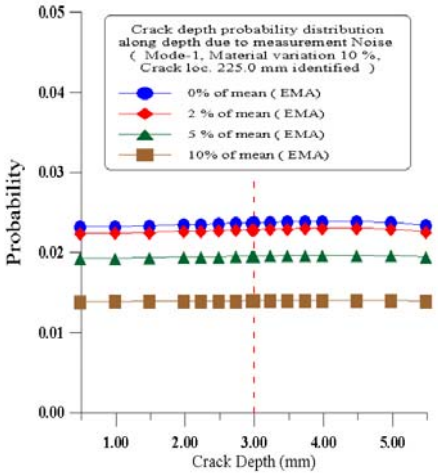

(c)10% material variation, mode 1

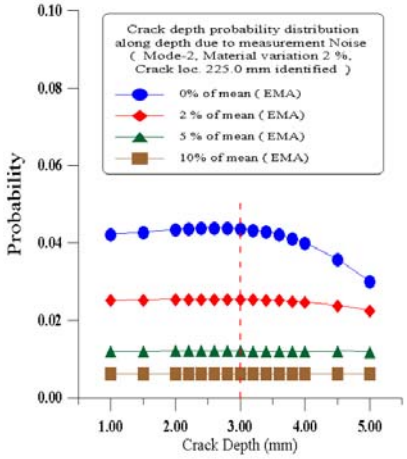

(d)2% material variation, mode 2

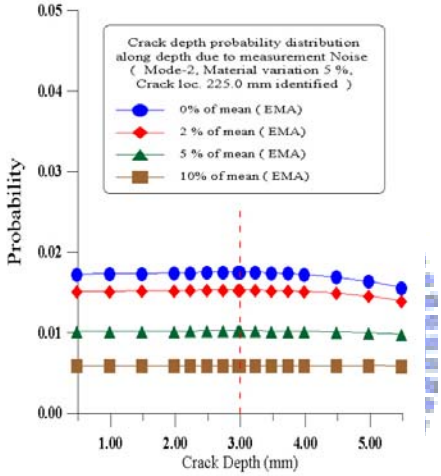

(e)5% material variation, mode 2

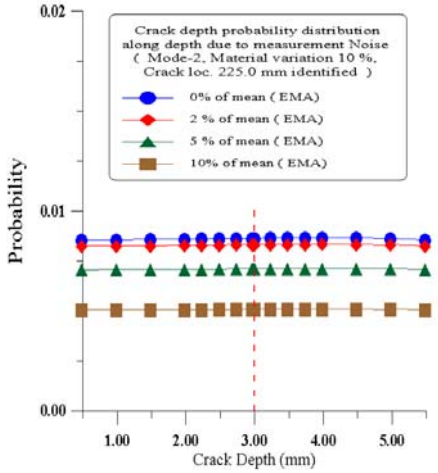

(f)10% material variation, mode 2

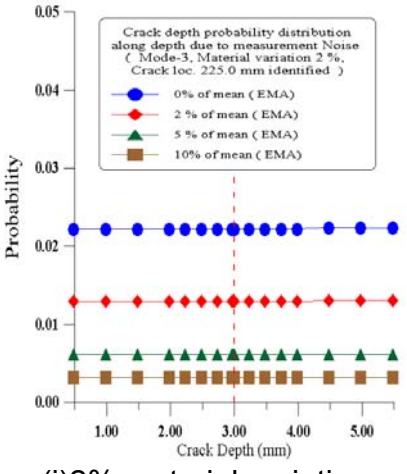

(i)2% material variation, mode 3

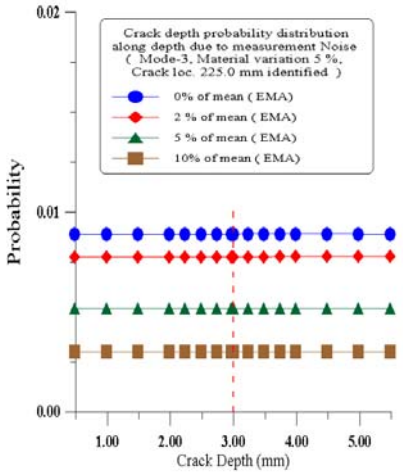

(j)5% material variation, mode 3

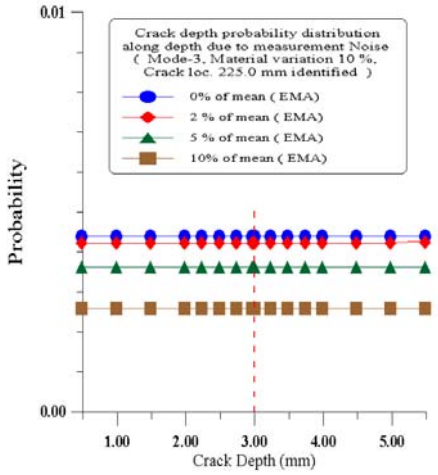

(k)10% material variation, mode 3

Figure 28. Probability distribution of Beam-N among varied crack depth
(Crk. Loc. 243mm, Dep. 3mm, Resol. 50mm)

5.6 The Multiple Cracks Example (Beam-M Case)

The assessment of above examples was all based on single crack configuration. Multiple cracks may exist in structure systems. In this section, the multiple cracks sample (named as Beam-M) was adopted to test for effectiveness of the proposed algorithm. For the convenient to compare with Beam-I, the authors made an extra crack on Beam-I, it was also manufactured by wild-cut at a new crack location 131mm with the crack depth 8mm. The Beam-M then has 2 cracks on its configuration that the first crack located at 131mm, depth 8mm plus the second crack located at 243mm, depth 10mm.

To review the results of EMA and finite element normal mode analysis, the cracks' location can be detected as shown in Fig. 29, from the peak of LDI index curve of the mode1 and 3; we found the cracks were located at 135mm(+3.05% error) and 245mm(+0.82% error), and there were different sensitivities on the peak of LDI for various modes. The averaged absolute error of multiple cracks was equal to +1.94%. With compared to Beam-I case (1.64% error), we have the same error level on crack location detection.

After we applying the identified multiple cracks location by LDI for FCI database generation (cracks location 135mm and 245mm). From EMA we have the first three modal frequencies 191.25Hz, 574.83Hz and 1079.46Hz of Beam-M and also from finite element analysis for no damage beam (Beam-S), its modal frequencies were 234.19Hz, 642.53Hz and 1251.1Hz. We have the frequencies change 18.34%, 10.54%, 13.72% for the three modes respectively. We need 2 sets of FCI curves to identify the depths due to the frequency change dominated by multiple cracks simultaneously. A little modification with compared to single crack case, we should first plot the contour lines of frequency change on each mode as shown in Fig. 30. Then by the intersection operation of two contour lines from different mode as shown in Fig. 31, the crack depths were identified as 8.00mm (0.0% error) and 9.90mm (+1.00% error) by the first and second mode or by the

first and third mode. The averaged absolute error for the depths of multiple cracks was equal to 0.50%. With compared to the results of Beam-I (2.07%), we also have the same error level on depth identification for multiple cracks case for the invariant system.

For the variant system with noised measurement, the statistical FCI database was also based on the cracks located at 135mm and 245mm that were detected by peak LDI. Various property variation and different level measurement noise applied, the crack depths were determined by the highest probability. As mention above, due the frequency change was dominated by multiple cracks simultaneously, we will determine all the depths at the same time. The probability of identified crack depths was represented by its brightness; the higher the probability, the brightened it was and vice versa. A red point in the figure indicated the highest probability on the depths. The assessed probability distributions of depths were shown in Fig. 32, 33 and 34 for mode 1, 2 and 3 respectively. The identified depths and its averaged absolutely error were list in Table 5.

Results from mode 1 as shown in the 1st column (2% material variation) and the 2nd column (5% material variation) in Fig. 32, its maximum probability of cracks' depth occurred at 8.50 mm and 9.90 mm for all levels of measurement noise. The maximum probability of cracks' depth occurred at 7.57 mm and 10.15 mm for all levels of measurement noise for 10% material variation as shown in the 3rd column in Fig. 32. In the 1st row of Table 5, we have found that their averaged absolute errors were ranged from 3.44% to 3.63% for mode 1. With compared to Beam-I single crack case (0.83% error for mode 1), we have acceptable error on the cracks' depth identified.

From mode 2 results, for 2% material variation (1st column in Fig. 33), the maximum probability of cracks' depth occurred at 7.50mm and 10.77mm for 0% and 2% measurement noise, the cracks' depth occurred at 8.25mm and 9.47mm for 5% and 10% measurement noise. For 5% material variation (2nd column in Fig.

33), the maximum probability of cracks' depth all occurred at 8.25mm and 9.47mm for all level measurement noise. For 10% material variation (3rd column in Fig. 33), the maximum probability of cracks' depth all occurred at 8.25mm and 10.33mm for all level measurement noise. In the 2nd row of Table 5, we found that their averaged absolute errors were ranged from 3.21% to 6.98% for mode 2. With compared to Beam-I single crack case (2.50% error for mode 2), we also have acceptable error on the crack depths identified.

From mode 3 results, for 2% material variation (1st column in Fig. 34), the maximum probability of cracks' depth occurred at 7.75mm and 10.33mm for all level measurement noise. For 5% material variation (2nd column in Fig. 34), the maximum probability of cracks' depth occurred at 8.50mm and 9.03mm for 0%, 2%, and 5% measurement noise, and occurred at 8.25mm and 9.47mm for 10% measurement noise. For 10% material variation (3rd column in Fig. 34), the maximum probability of cracks' depth all occurred at 7.00mm and 11.63mm for all level measurement noise. In the 3rd row of Table 5, we found that their averaged absolute errors were ranged from 3.21% to 14.40% for mode 3. With compared to Beam-I single crack case (2.50% error for mode 3), we have the larger error on the cracks' depth identified.

Observation from Fig. 32, 33 and 34, we have the same conclusion that the result from the lower mode, the lower material variant and the lower noise in measurement, we will have the brightened (sharpest) peak and the narrowest spreading on its probability distribution on cracks' depth identification.

Table 5. Peak Probability among Material Variation with Different Level Measurement Noise

Mode No.	EMA Measure Noise	Material Variation (Mass Density & Young's Modulus)								
		σ= ±2% μ			σ= ±5% μ			σ= ±10 % μ		
		Depth.(mm)		Avg. Err. of 2-Crks (%)	Depth.(mm)		Avg. Err. of 2-Crks (%)	Depth.(mm)		Avg. Err. of 2-Crks (%)
		Crk-1	Crk-2		Crk-1	Crk-2		Crk-1	Crk-2	
1	0 %μ	8.50	9.90	3.63	8.50	9.90	3.63	7.57	10.15	3.44
	±2%μ	8.50	9.90	3.63	8.50	9.90	3.63	7.57	10.15	3.44
	±5%μ	8.50	9.90	3.63	8.50	9.90	3.63	7.57	10.15	3.44
	±10%μ	8.50	9.90	3.63	8.50	9.90	3.63	7.57	10.15	3.44
2	0 %μ	7.50	10.77	6.98	8.25	9.47	4.21	8.25	10.33	3.21
	±2%μ	7.50	10.77	6.98	8.25	9.47	4.21	8.25	10.33	3.21
	±5%μ	8.25	9.47	4.21	8.25	9.47	4.21	8.25	10.33	3.21
	±10%μ	8.25	9.47	4.21	8.25	9.47	4.21	8.25	10.33	3.21
3	0 %μ	7.75	10.33	3.21	8.50	9.03	7.98	7.00	11.63	14.40
	±2%μ	7.75	10.33	3.21	8.50	9.03	7.98	7.00	11.63	14.40
	±5%μ	7.75	10.33	3.21	8.50	9.03	7.98	7.00	11.63	14.40
	±10%μ	7.75	10.33	3.21	8.25	9.47	4.21	7.00	11.63	14.40

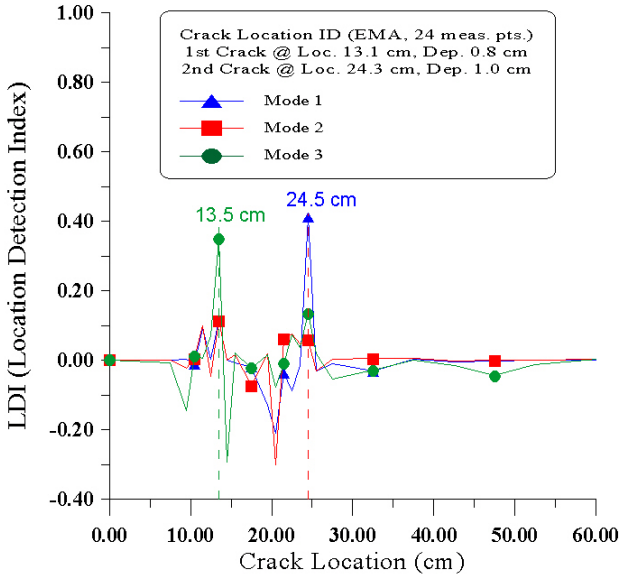

Figure 29. Multiple Cracks Location Detect by LDI
(Crk-1 loc.131mm, Crk-1 Dep. 8mm, Crk-2 loc.243mm, Crk-2 Dep. 10mm)

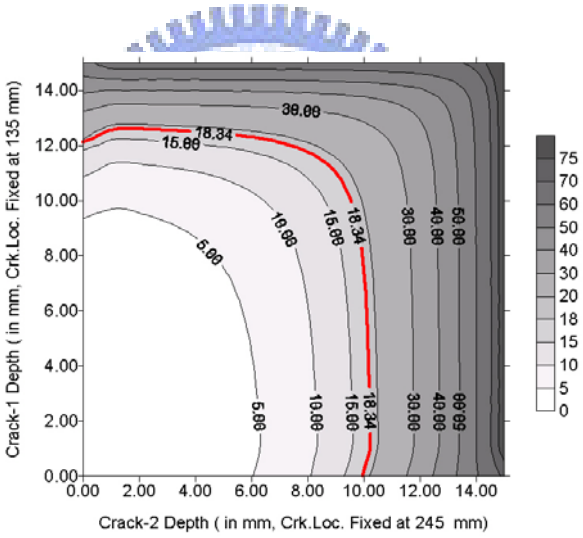

(a) mode 1 (18.34%)

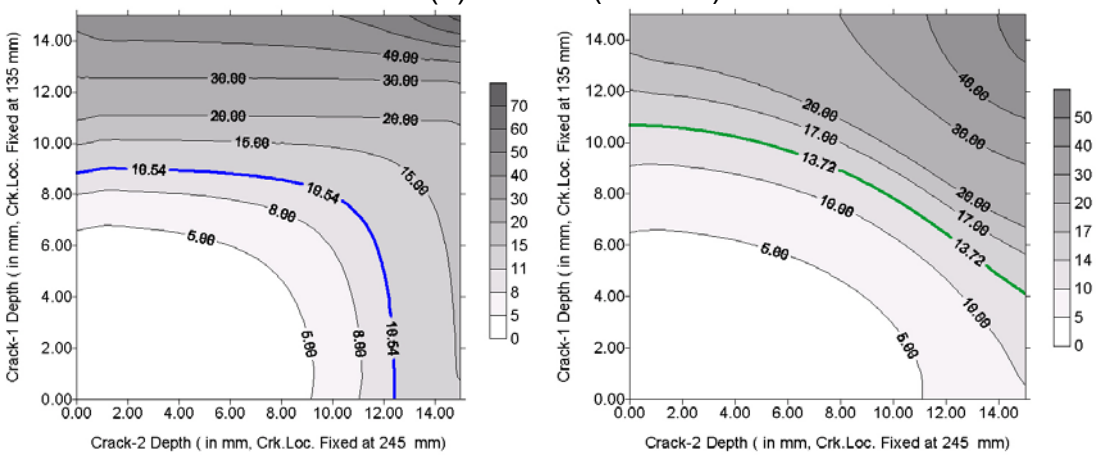

(b) Mode 2 (10.54%) (c) Mode 3 (13.72%)

Figure 30. FCI Contour Lines due to multiple cracks existence

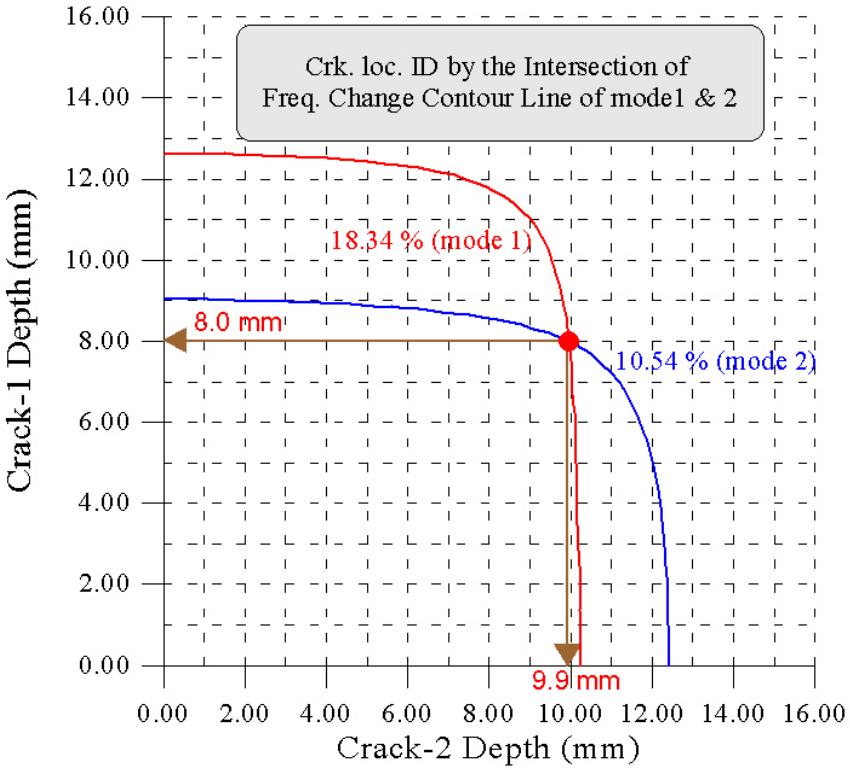

(a) by Mode 1 and 2

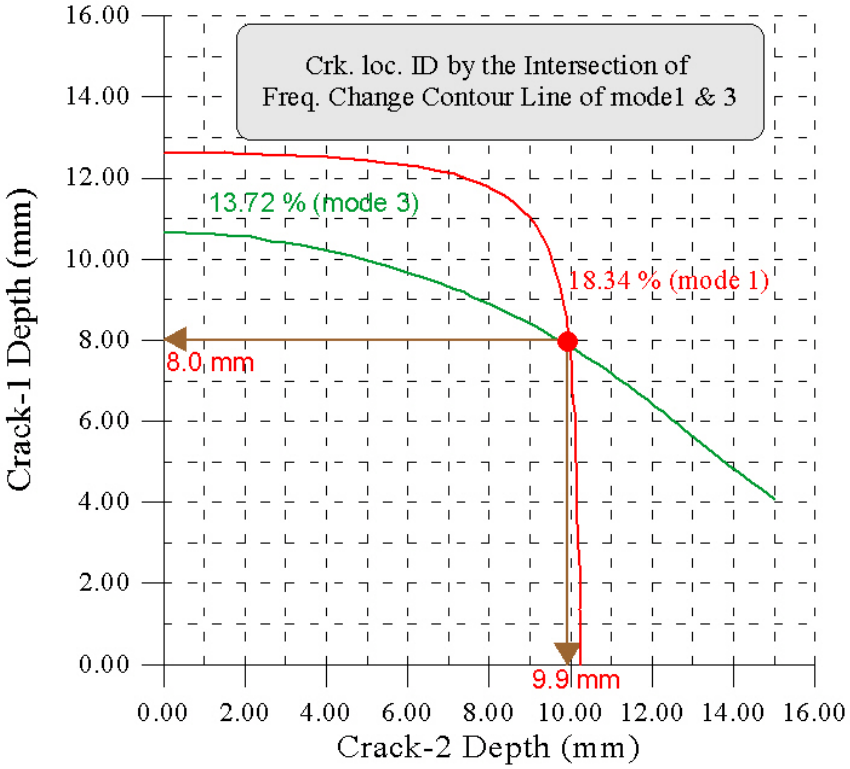

(b) by Mode 1 and 3

Figure 31. Crack depths identification by the intersection of two FCI contour lines

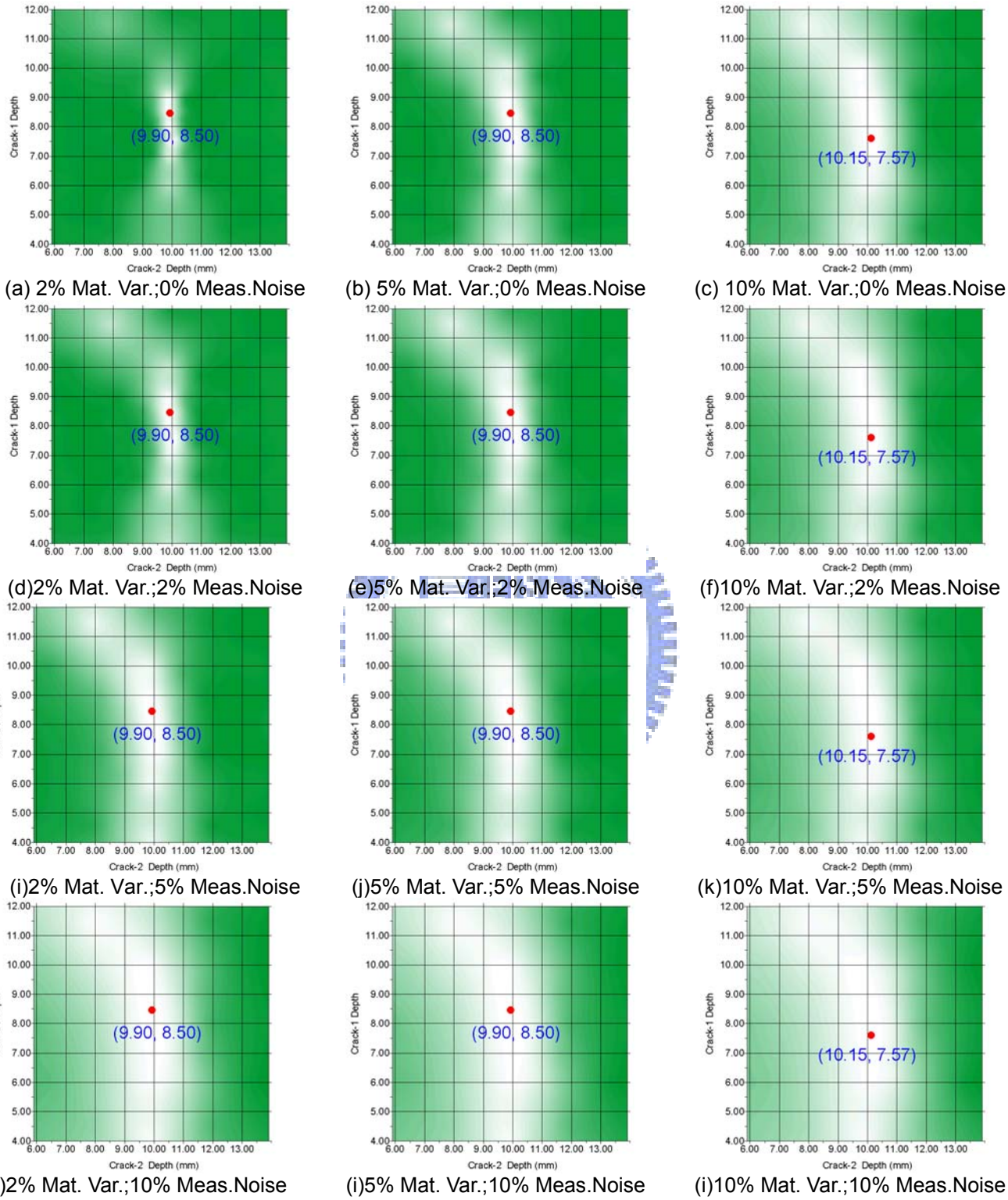

(a) 2% Mat. Var.;0% Meas.Noise (b) 5% Mat. Var.;0% Meas.Noise (c) 10% Mat. Var.;0% Meas.Noise

(d)2% Mat. Var.;2% Meas.Noise (e)5% Mat. Var.;2% Meas.Noise (f)10% Mat. Var.;2% Meas.Noise

(i)2% Mat. Var.;5% Meas.Noise (j)5% Mat. Var.;5% Meas.Noise (k)10% Mat. Var.;5% Meas.Noise

(i)2% Mat. Var.;10% Meas.Noise (i)5% Mat. Var.;10% Meas.Noise (i)10% Mat. Var.;10% Meas.Noise

Figure 32. Probability distribution of crack depths by <u>mode 1</u>
(Crk.-1 Loc. 243mm, Dep. 8mm, Crk.-2 Loc. 243mm, Dep. 10mm)

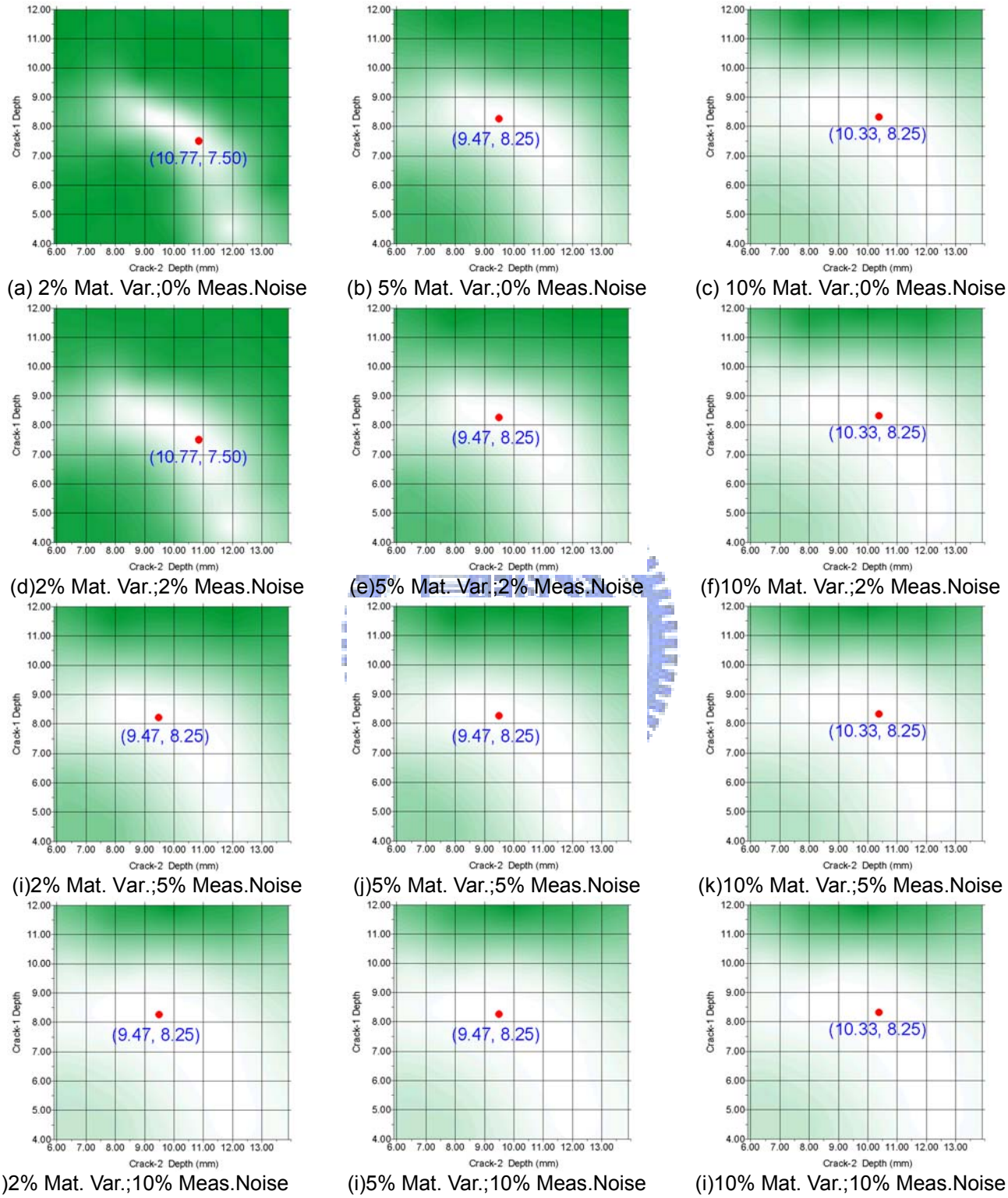

(a) 2% Mat. Var.;0% Meas.Noise (b) 5% Mat. Var.;0% Meas.Noise (c) 10% Mat. Var.;0% Meas.Noise

(d)2% Mat. Var.;2% Meas.Noise (e)5% Mat. Var.;2% Meas.Noise (f)10% Mat. Var.;2% Meas.Noise

(i)2% Mat. Var.;5% Meas.Noise (j)5% Mat. Var.;5% Meas.Noise (k)10% Mat. Var.;5% Meas.Noise

(i)2% Mat. Var.;10% Meas.Noise (i)5% Mat. Var.;10% Meas.Noise (i)10% Mat. Var.;10% Meas.Noise

Figure 33. Probability distribution of crack depths by <u>mode 2</u>
(Crk.-1 Loc. 243mm, Dep. 8mm, Crk.-2 Loc. 243mm, Dep. 10mm)

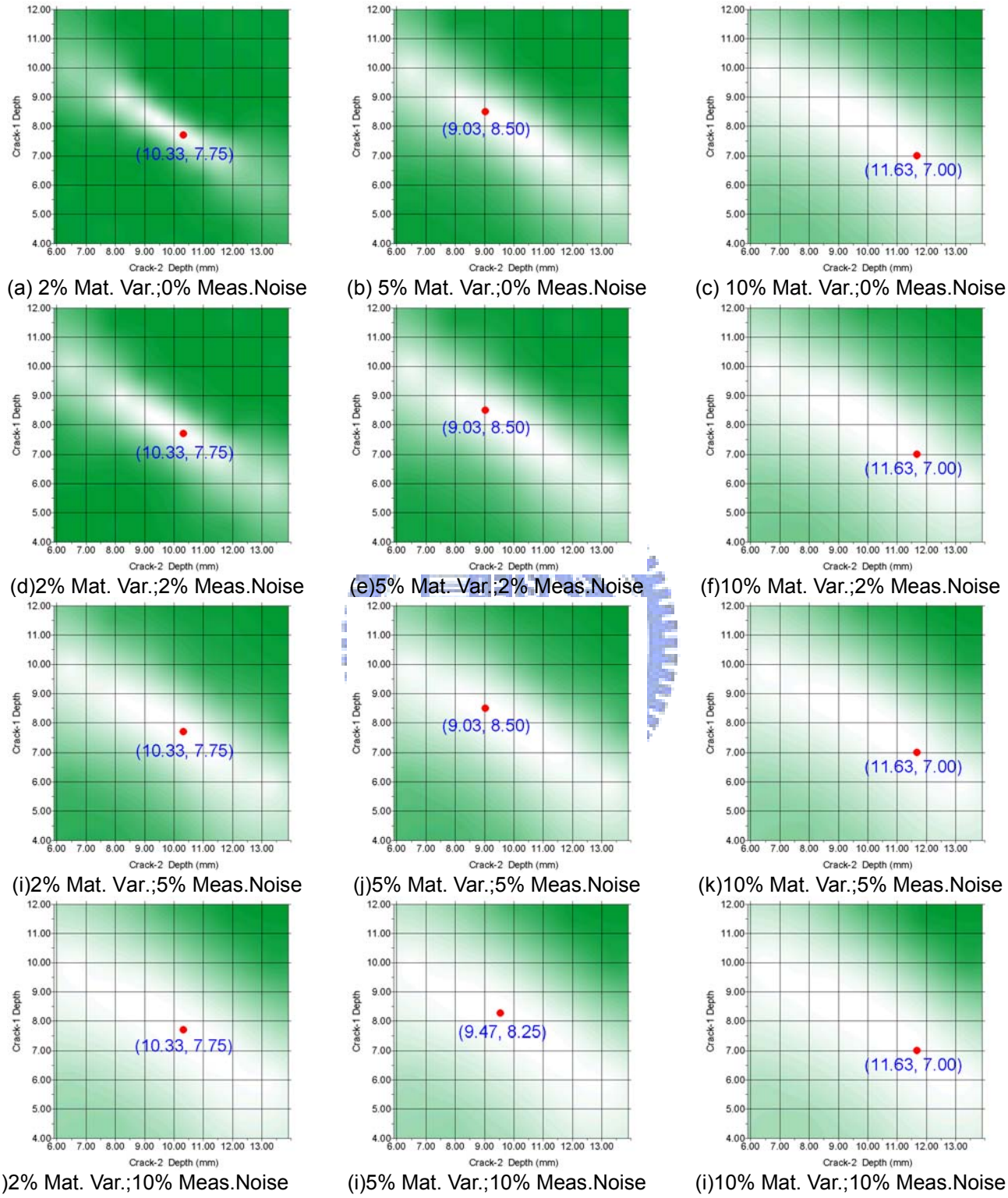

(a) 2% Mat. Var.;0% Meas.Noise (b) 5% Mat. Var.;0% Meas.Noise (c) 10% Mat. Var.;0% Meas.Noise

(d)2% Mat. Var.;2% Meas.Noise (e)5% Mat. Var.;2% Meas.Noise (f)10% Mat. Var.;2% Meas.Noise

(i)2% Mat. Var.;5% Meas.Noise (j)5% Mat. Var.;5% Meas.Noise (k)10% Mat. Var.;5% Meas.Noise

(i)2% Mat. Var.;10% Meas.Noise (i)5% Mat. Var.;10% Meas.Noise (i)10% Mat. Var.;10% Meas.Noise

Figure 34. Probability distribution of crack depths by <u>Mode 3</u>
(Crk.-1 Loc. 243mm, Dep. 8mm, Crk.-2 Loc. 243mm, Dep. 10mm)

CHAPTER 6
Conclusions and Discussions

In the presented research, we have the conclusions and discussion as follows:

(1) A damage assessment algorithm was developed by introducing the Monte Carlo statistical process and the modeling of material variations, measurement noise by Gaussian model. The algorithm has been verified by single and multiple cracks in a uniform mass density and Young's modulus variations system which is incorporated with different level noise in modal frequency measured. The effects on measurement resolution and the shallow depth crack characteristic were also investigated.

(2) Due to the material variation of the beams were varied uniformly across the entire beam, the LDI index for crack location detection was hold for both the property variant and invariant system. For the middle depth single crack beam (Beam-I, 10/16 depth of structure) we have the averaged absolute error 1.64% on the basis of measurement resolution 1/60 in beam length near the crack zone and 5/60~7.5/60 on the others, 18-impact locations in total.

(3) The crack depth was determined by the FCI index or the statistical FCI database. For the middle depth single crack beam (Beam-I) on appropriate measurement spacing, we have the averaged absolute error 2.07% for the invariant system and 1.94% error for variant system with material variation, measurement noise least than 10%.

(4) For practical applications, the 'fixed response' method of EMA should be change to 'fixed impact' to save labor work. It would be adequate to use a non-uniform spacing between measurement points and apply 1%~2% spacing in beam length close to the crack, 8%~13% in spacing for the others.

To increase the spacing from 1/60(Beam-I) to 5/60 (Beam-N) in beam length on the crack zone, the error will be increased to 4.52 times in crack location detection, to 4.25 times in crack depth for property invariant system, and to 4.51 times in depth for property variant system.

(5) For the shallow crack depth single crack example (Beam-N, 3/16 depth of structure), the LDI index works well for location detection. With compared to the result of middle depth single cracked beam (Beam-I, 10/16 depth of structure), the error will be increased to 3.18 times in location detection, to 5.82 times in depth identification for property invariant system by mode 1 and 2 data, and to3.44 times for property variant system by mode 1 data under 2% material variations with no measurement noise.

(6) The LDI index works well for the location detection of multiple cracks example (Beam-M case). We have the averaged absolute error 1.94% based on 18-impact locations measurement. The FCI and statistical FCI database works well too, we have the averaged absolute error 0.50% for the invariant system and about 5.37% error for system with material variation, measurement noise least than 10%.

(7) For unknown damage system with property variant and noised frequency measurements, we should apply the lower mode for crack depth assessment to achieve better solution. By applying the lower modal data, we should have the higher probability and confirmation in the severity identification.

(8) The pre-set resolution of FCI and statistical FCI database will affect the accuracy of depth identification. In the research, for single crack case the resolution was ranged from 2.5% to 6.7% in beam depth, 0.30% to 2.5% for multiple cracks case; it should be adjusted appropriately by specific requirements or by the engineering practice.

(9) In the research, the authors have model the beams in free-free boundary. Further study will be required for structure member other than free-free type. It can be expected that the LDI process for crack location is based on measurement data of real structure, the algorithm is still suitable for non-free-free boundary condition, but for the FCI process from simulation database for the crack depth assessment, we need to deal with the stiffness identification for imperfect boundary condition before building the database.

(10) Although the authors have completed fundamental study of proposed algorithm in vibration laboratory, there is still need study efforts in non-rectangular cross section beam, for how to increase the robustness of proposed algorithm for the larger material variation, the measurement noise, and also for the adaptation and verification work for real engineering practice.

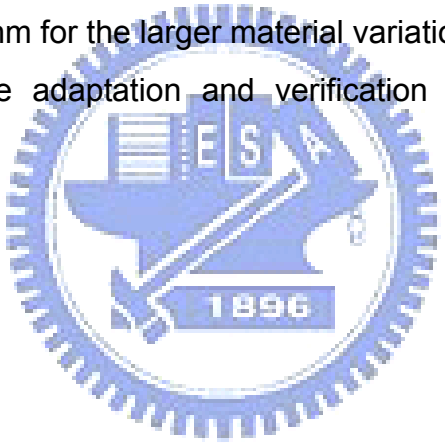

References：

[1] Allemang, R. J., “Brown DL. A Correlation Coefficient for Modal Vector Analysis”, Proceeding of 1st International Modal Analysis Conference, pp. 110-116, 1983.

[2] Bahlous, S. El-Ouafi, Smaoui, H., and El-Borgi, S., ”Experimental Validation of An Ambient Vibration-based Multiple Damage Identification Method Using Statistical Modal Filtering”, Journal of Sound and Vibration 325(1), pp.49-68, 2009.

[3] Barsoum, R. S., “A Degenerate Solid Element for Linear Fracture Analysis of Plate Bending and General Shells”, International Journal of Numerical Method in Engineering, 10, pp.551-564, 1976.

[4] Cawley, P., Adams, R. D., “The location of defects in structures from measurements of natural frequencies”, Journal of Strain Analysis , 14(2), pp. 49-57, 1979.

[5] Clough, R. W. and Penzien, J., Dynamics of Structures, 2nd ed. Singapore: McGraw-Hill Book Co, pp. 184-189, 1993.

[6] Cornwell, P., Farrar, C. R., Doebling, S. W., Sohn, H., “Environmental variability of modal properties”, Experimental Techniques, 23(6), pp. 45-48. 1999.

[7] Deraemaeker, A., Reynders, E., De Roeck, G., Kullaa, J., ”Vibration-based structural health monitoring using output-only measurements under changing environment”, Mechanical Systems and Signal Processing, 22(1), pp. 34-56, 2008.

[8] Dobeling, S. W., Farrar, C. R., Prime, M. B., Shevitz, D. W., Damage Identification and Health Monitoring of Structural and Mechanical Systems from Changes in Their Vibration Characteristics: A Literature Review. Los Alamos National Laboratory Report, LA-13070-MS, 1996.

[9] Doebling, S. W., Farrar, C. F., “Statistical damage identification techniques applied to the I-40 bridge over the Rio Grande River”, Proceeding of 16th International Modal Analysis Conference, pp. 1717-1724, 1998.

[10] Efron, B., Tibshirani, R., An Introduction to the Bootstrap. in Applied Monographs on Statistics and Applied Probability 57, Chapman and Hall, 1993.

[11] Ewins, D. J., Modal Testing: Theory and Practice, 1st ed. Singapore: John Wiley & Sons Inc., 1984

[12] Freund, J., Mathematical statistics, 5th ed. Englewood Cliffs, N.J: Prentice Hall, pp. 462, 1992.

[13] Furukawa, A., Otsuka, H., “Strutural Damage Detection Method Using Uncertain Frequency Response Functions”, Computer-Aided Civil and Infrastructure Engineering, 21, pp. 292-305, 2006.

[14] Ko, J. M., Wang, J. Y., Ni, Y. Q., Chak, K. K., “Observation on Environmental Variability of Modal Properties of a Cable-Stayed Bridge from One-Year Monitoring Data”, Fu-Kuo Chang(ed.), Structural health monitoring 2003, Proc. 4th IWSHM, Lancaster: DEStech; 15-17 Sept., pp. 467-474, 2003.

[15] Lin, R.-J. and Cheng, F.-P., “A Damage Detection Approach Considering the Stiffness and Mass Variations”, in Ou, Li & Duan (ed.), The 2nd International Conference on Structural Health Monitoring of Intelligent Infrastructure (SHMII-2’2005), pp. 839-844, Nov.16-18, Shenzhen, P. R. of China, 2005

[16] Lin, R.-J. and Cheng, F.-P., “A Damage Detection Approach for Structures with Natural Frequency Variations”, in Fu-Kuo Chang(ed.), Structural health monitoring 2005, Proc. 5th IWSHM, Standford, CA., pp. 1139-1146, Sept. 12-14, 2005

[17] Mckay, M. D., Beckman, R. J., Conover WJ. “A Comparison of Three Methods for Selecting values of Input Variables in the Analysis of Output from a Computer Code”. Technometrics , 21(2), pp. 239-245, 1979.

[18] Oh, C. K. and Sohn, H., ”Damage Diagnosis under Environmental and Operational Variations Using Unsupervised Support Vector Machine”, Journal of Sound and Vibration, 325(1), pp. 224-239, 2009.

[19] Olsson, A., Sanberg, G., Dahlblom, O., “On the Latin hypercube sampling for structural reliability analysis” , Structure Safety , 25, pp. 47–68, 2003.

[20] Owen, D. R. J. and Fawkes, A. J., Engineering Fracture Mechanics, Swansea, U. K., Pineridge Press Ltd, pp. 62-67, 1983.

[21] Pandey, A. K., Biswas, M., Samman MM. ”Damage Detection from Changes in Curvature Mode Shape”, Journal of Sound and Vibration,145(2), pp. 321-332,1991.

[22] Park, J.-H., Kim, J.-T., Hong, D.-S., Ho, D.-D., and Yi, J.-H., ”Sequential Damage Detection Approaches for Beams Using Time-modal Features and Artificial Neural Networks”, Journal of Sound and Vibration, 323(1), pp. 451-474, 2009.

[23] Peeters, B., Roeck, G. De. “One-year monitoring of the Z24-Bridge: Environmental effects versus damage events”, Earthquake Engineering and Structural Dynamics, 30, pp. 149-171, 2001.

[24] Press, W. H., Teukolsky, S. A., Vetterling, W. T., Flannery BP. Numerical Recipes in Fortran, 2nd ed. Cambridge University Press, Section 15.6, 1992.

[25] Rizos, D. D., Fassois, S. D., Marioli-Riga, Z. P., and Karanika, A. N., "Vibration-based Skin Damage Statistical Detection and Restoration Assessment in a Stiffened Aircraft Panel", Mechanical Systems and Signal Processing, 22(2), pp. 315-337, 2008.

[26] Sikorsky, C., Stubbs, N., Guan, F., "The Impact of Natural Frequency Variation on Damage Detection". in: Fu-Kuo Chang(ed.), Structural health monitoring 2003, Proc. 4th IWSHM, Lancaster:DEStech; 15-17 Sept., pp. 701-708, 2003.

[27] Sohn, H., Dzwonczyk, M., Straser, E. G., Kiremidjian AS , Law KH, Meng T. "An experimental study of temperature effect on modal parameters of the Alamosa Canyon Bridge", Earthquake Engineering and Structural Dynamics , 28(8), pp. 879-897, 1999.

[28] Sohn, H., Farrar, C. R., Hemez, F. M., Shunk, D. D., Stinemates, D. W., Nadler, B. R., A Review of Structural Health Monitoring Literature: 1996-2001. Los Alamos National Laboratory Report, LA-13976-MS, 2003.

[29] Stein, M., "Large Sample Properties of Simulations Using Latin Hypercube Sampling", Technometrics , 29(2), pp.143-151, 1987.

[30] Wang, B. S., and He, Z. C., "Crack detection of arch dam using statistical neural network based on the reductions of natural frequencies", Journal of Sound and Vibration, 302(4), pp. 1037-47, 2007.

[31] Xia, Y., Hao, H., "Statistical Damage Identification of Structures with Frequency Changes", Journal of Sound and Vibration, 63(2), pp. 853-870, 2003.

[32] Xia, Y., Hao, H., Zanardo, G., Deeks, A., "Long term vibration monitoring of an RC slab-Temperature and humidity effect", Engineering Structures, 28, pp. 441–452, 2006.

[33] Zhang, Q. W., "Statistical Damage Identification for Bridges Using Ambient Vibration Data", Computers and Structures, 85(7), pp. 476-485, 2007.

[34] Zienkiewicz, O. C., The Finite Element Method:vol-II, 4th ed. Singapore: McGraw-Hill Book Co., pp. 159-167, 1989.

[35] Zienkiewicz, O. C., The Finite Element Method:vol-I, 4th ed. Singapore: McGraw-Hill Book Co., pp. 23-30, 1989.